High-dimensional Bayesian nonparanormal dynamic conditional model with multivariate volatility applications*

Hayun Song†

This version: November 17, 2023

Abstract

This paper proposes a Bayesian approach for the estimation of large conditional precision matrices instead of inverting conditional covariance matrices estimated using, for example, the dynamic conditional correlations (DCC) approach. By adopting a Wishart distribution and horseshoe priors within a DCC–GARCH(1,1) model, our method imposes sparsity and circumvents the inversion of conditional covariance matrices. We also employ a nonparanormal method with rank transformation to allow for conditional dependence without estimating transformation functions to achieve Gaussianity. Monte Carlo simulations show that our approach is effective at estimating the conditional precision matrix, particularly when the number of variables (N) exceeds the number of observations (T). We investigate the utility of our proposed approach with two real-world applications. First, to study conditional partial correlations among international stock price indices. Second, to test for $\boldsymbol{\alpha}$ in the context of CAPM and Fama-French 5 factor models with a conditional precision matrix-based Wald-type test. The results indicate stable conditional partial correlations through market disruptions. When there are market disruptions, blue chip stocks chosen from S&P 500 daily returns provide statistically significant evidence against the CAPM and Fama-French five models.

Keywords: High-dimensional multivariate volatility, Bayesian estimation, Precision matrix, Conditional partial correlations, Nonparanormal model, Semiparametric model

JEL Classification Codes: C11, C32, C58

*I am especially grateful to my adviser Hashem Pesaran, Cheng Hsaio, and Timothy Armstrong for their continuous advice and support. All mistakes are my own.

†Department Economics, University of Southern California, Ph.D. Candidate; Correspondence: hayunson@usc.edu.

1 Introduction

Volatility modeling plays an important role in financial econometrics. Early research focused on univariate volatility models, such as autoregressive conditional heteroskedasticity (ARCH, Engle 1982) and generalized ARCH (GARCH) proposed by Bollerslev (1986). More recently, with increasing interconnection in financial markets and the advent of high-frequency, high-dimensional data have necessitated the transition toward multivariate volatility models. These models capture the dynamic correlations and covariances among multiple assets, providing a more suitable framework for portfolio selection and optimization (Ledoit and Wolf, 2003, 2017), testing capital asset pricing models (Sentana, 2009), and risk management strategies (Fan, Zhang, and Yu, 2012). However, the estimation of covariance matrices in this multivariate context is subject to the curse of dimensionality, where the number of parameters can exceed the number of available time series observations.

To address the challenges associated with the estimation of covariance matrices in high-dimensional contexts, a large body of literature that focuses on improving the estimation of large covariance matrices through shrinkage and regularization methods (Ledoit and Wolf, 2004a,b) has emerged. These techniques, which began with linear shrinkage and have since incorporated nonlinear variants (Ledoit and Wolf, 2012, 2017, 2020, 2022; Engle, Ledoit, and Wolf, 2019; Nard, Engle, Ledoit, and Wolf, 2022), have proved important for error minimization and portfolio optimization. Researchers have also extended these methods to dynamic models, such as the DCC with a linear (DCC–L) and nonlinear (DCC–NL) shrinkage framework (Engle, Ledoit, and Wolf, 2019; Pakel, Shephard, Sheppard, and Engle, 2021), and embraced sparsity-promoting approaches like banding and thresholding (Bickel and Levina, 2008; Rothman, Levina, and Zhu, 2009; Cai and Liu, 2011; Bailey, Pesaran, and Smith, 2019). Fan, Liao, and Mincheva (2013) further assert the effectiveness of regularization for precision matrix estimation under certain factor structures with consistent convergence rates. Additionally, dynamic covariance models (DCMs) that leverage kernel smoothing have been introduced (Chen and Leng, 2016) alongside semiparametric extensions for high-dimensional settings (Chen, Li, and Linton, 2019). Poignard and Asai (2023) explored high-dimensional variance-covariance modeling within the multivariate stochastic volatility (MSV) framework using a penalized OLS framework without relying on Monte Carlo Markov Chain (MCMC) by introducing a vector autoregressive and moving-average (VARMA) representation for MSV.

This paper studies the estimation of conditional precision matrices in high-dimensional settings within the DCC framework, essential for financial applications that require estimation of the inverse of the covariance matrix[1]. In carrying out this research, we face two difficulties.

[1]To clarify, we differentiate between two types of matrices: those that are static and those that are dynamic. For simplicity, we will call the dynamic ones '*conditional matrices*' and the static ones '*unconditional matrices*.' This distinction is important because it reflects whether the matrix elements are fixed (without subscript t) or

First, we cannot employ the conventional DCC framework by merely inverting its components because it results in a matrix that is, at best, semi-positive definite. Furthermore, inverting the unconditional component is ill-conditioned when the number of variables (N) is larger than the number of time series observations (T). Second, suppose we can extract conditional precision matrices from the DCC framework. In that case, the resulting conditional partial correlations derived from the conditional precision matrices only interpret conditional independence within the restriction of a multivariate Gaussian distribution, an assumption which is rarely met in finance and macroeconomic analyses. Moreover, even if we use the rank transformation to convert the dataset to follow a Gaussian distribution, such as the Copula, quantile, and standard nonparanormal model, it does not retain the scale of the conditional precision matrices. This scale distortion leads to an identification problem, where multiple precision matrices may correspond to the same inverse correlation matrix. Accordingly, our focus is on exploring the advantages of directly estimating precision matrices, particularly in addressing the identification challenges, as opposed to relying on the inversion of estimated conditional covariance matrices.

We make two main contributions to the literature of high-dimensional multivariate volatility modeling, namely the estimation of conditional precision matrices exploring the possibility of conditional dependence. The first is the development of a Bayesian method for the estimation of the conditional precision matrix within the high-dimensional DCC–multivariate GARCH (MGARCH) framework instead of inverting the estimated conditional covariance matrix. We use a Bayesian approach that samples from the Wishart distribution to bypass the challenges of inverting semi-positive definite matrices. The estimation is carried out using the Metropolis-Hastings within the Gibbs sampling algorithm. While DCC–MGARCH models perform well for a moderate number of assets (typically fewer than 25), they struggle with larger datasets due to the computational demands of estimating the unconditional precision matrix, $\mathbf{\Omega}$. For a dataset with T time periods and N assets, using a sample covariance matrix necessitates estimating $N(N-1)/2$ parameters, which is prone to considerable error unless $T \gg N$. To address this problem, we estimate $\mathbf{\Omega}$ using the Cholesky decomposition $\mathbf{\Omega} = \mathbf{L}\mathbf{L}'$, where $\mathbf{L}$ is a lower triangular matrix. In the DCC framework, we apply a horseshoe prior to introduce sparsity on $\mathbf{\Omega}$, as outlined in the approach by Neville, Ormerod, and Wand (2014). Additionally, we incorporate block updates in our proposed distributions to achieve a balance between computational efficiency and accuracy.

Our second contribution is to provide estimates of both conditional precision, $\mathbf{P}_t = (p_{ij,t})$, and partial correlation $\mathbf{\Psi}_t = (\psi_{ij,t})$ matrices aimed at achieving volatility interconnectedness interpretation. We achieve this utilizing a Bayesian nonparanormal framework that applies a rank transformation, converting non-Gaussian distributions to approximate Gaussian ones. The standard nonparanormal estimation process approximates an unknown data distribution with

change over time (with subscript t).

a Gaussian distribution by transforming original variables using a smooth, monotonic function, thus achieving a Gaussian approximation. In contrast, the rank transformation approach, which we employ, simplifies this process. It bypasses the intensive computation required to estimate transformation functions. Moreover, by providing the DCC-MGARCH structure, we can identify $\mathbf{P}_t$ from the inverse correlation matrix $\mathbf{S}_t = (s_{ij,t})$ given the conditional variances as specified by the univariate GARCH procedures. Under Gaussian distributions, the relationship between $\mathbf{P}_t$ and $\mathbf{S}_t$ can be established using the diagonal elements of the conditional covariance matrices: $p_{ij,t} = s_{ij,t}\sqrt{(1/\sigma_{ii,t})(1/\sigma_{jj,t})}$, where $\sigma_{ii,t}$ is the conditional variance modeled on a univariate GARCH process for security i (Rue and Held, 2005, p.26). Thus, with precise estimation of univariate GARCH processes for each security variable and a Gaussian approximation, we obtain conditional precision matrices suitable for the DCC-MGARCH model. This method circumvents the inversion of the entire conditional covariance matrices, a step often required under conventional DCC approaches.

Nonparanormal model, nonparanormal estimation was introduced as a semiparametric extension of Gaussian graphical models with the capability to capture non-Gaussian marginal distributions through smooth, monotonic transformations (Liu, Lafferty, and Wasserman, 2009). Subsequent developments in this line of inquiry have addressed high-dimensional settings in the Bayesian nonparanormal graphical model (Mulgrave and Ghosal, 2020, 2022, 2023). Therefore, our paper can add to the literature on high-dimensional multivariate volatility, introducing a Bayesian nonparanormal approach to approximate unknown distributions to normality and develop rank likelihood for constructing sparse precision matrices. This approach synergizes with the DCC framework, which comprises a univariate GARCH process for volatility prediction and a correlation estimation based on standardized residuals.

We conduct a number of Monte Carlo (MC) simulations to evaluate the performance of the Bayesian nonparanormal conditional estimator and compared it with existing methods for estimating conditional precision matrices from the literature. Our study involves two simulation designs: the first design generates conditional precision matrices with a narrow range of eigenvalues, suggesting numerical stability, while the second design produces matrices with widely varying eigenvalues, typically pointing to numerical instability. In the first simulation design, our Bayesian estimator outperforms DCC-L, DCC-NL, Gaussian, and t-Copula models (Patton, 2009) in estimating conditional precision matrices for 20 different sample size combinations, $T \in \{50, 100, 150, 200, 250\}$ and $N = \{25, 50, 100, 125\}$, in terms of spectral and Frobenius norms. Although the extent of this outperformance, measured by the ratio of norm loss averages (RNLA), diminishes as sample size, T, and the number of variables, N, increase, our methods show improved performance over DCC-L and DCC-NL in estimating conditional correlation matrices when sample size and the number of variables increase, but not against Gaussian and t-Copula models. In the second MC design, all considered estimators, including

our own, struggle with estimating conditional precision matrices due to instability in the eigenvalue distribution. However, for inverse correlation matrices, our method slightly outperforms DCC-N and DCC-NL as N and T increase, and outperforms both the Gaussian and t-Copula methods. As in the first design, this advantage diminishes with larger T values compared to the Gaussian and t-Copula for all sample size combinations.

We employ our proposed method in two empirical applications: daily foreign stock price indices and returns on blue chip stocks selected based on the market capitalization from the Standard and Poor (S&P) 500 in the U.S. equity market. In analyzing foreign stock indices over the period January 4, 1991, to August 31, 2023, we focus on deciphering their complex interdependencies through conditional partial correlations. We evaluate conditional correlations to understand how pairs of variables are linked under financial market disruptions. However, conditional partial correlations are crucial for deeper insights into international market dynamics. They isolate specific relationships by excluding global and region-specific influences, clarifying interactions between specific pairs of individual stocks or sectors. It is also important in conditional covariance analysis of these indices, as it separates direct variable relationships from the myriad of influencing local and global factors, thereby offering a different viewpoint in understanding the variables' interactions. We find that the range of the conditional partial correlations is narrower than the associated conditional correlations. Furthermore, the overall average of the pair-wise relations is smaller than the conditional correlations. Under financial market disruptions, the relationship of the indices exhibits weakened mean values and reduced variances, denoting a more stable behavior even under stressful market conditions.

When examining selected securities based on the market capitalization in S&P 500 over the period September 2, 2016, to July 31, 2023, we test asset pricing theory where, in an ideal, frictionless market, a financial asset's excess return is determined by the product of its factor loadings and the excess returns of corresponding risk factors, plus a random component. Testing the theory involves estimating precision matrices used in Wald-type statistical tests for evaluating asset pricing models. We assess the robustness of our method by applying it to various test statistics in the context of the consumption asset pricing model (CAPM) and Fama-French 5 factor model over different time frames, including periods of market turmoil, and by comparing it with the $\hat{J}_\alpha$ test by Pesaran and Yamagata (2023), which does not involve the precision matrix. Using our proposed conditional precision matrices, we find that the Wald statistic rejects $\mathbb{H}_0 : \boldsymbol{\alpha} = 0$, mainly during periods of major market disruptions, COVID-19, and FED's inflation containment rate hikes periods. All test statistics show similar results for the market disruption periods except for COVID-19.

Our paper adds to the literature on the Copula model and nonparanormal estimation. In the context of the Copula model, its application has become recognized as a versatile framework for capturing a diverse range of dependency structures, encompassing both linear and tail depen-

dencies (Patton, 2009; Aas, Czado, Frigessi, and Bakken, 2009; Anatolyev and Pyrlik, 2022). Subsequent advancements in the domain have yielded specific models such as the pair copula constructions (PCC) (Müller and Czado, 2019a), vine copulas (Müller and Czado, 2019b), and Gaussian copula graphical models (GCGM) (Pitt, Chan, and Kohn, 2006; Dobra and Lenkoski, 2011; Liu, Han, Yuan, Lafferty, and Wasserman, 2012; Mohammadi, Abegaz, Heuvel, and Wit, 2017). These specialized models facilitate the scrutiny of ultra-high-dimensional data with complex interdependencies. Furthermore, the utility of copula methods has been expanded to accommodate dynamic dependencies through the incorporation of DCC frameworks (Kim and Jung, 2016; Oh and Patton, 2016, 2017, 2023). However, despite their versatility, copula models often presuppose rigid functional forms for dependencies, which may misalign with empirical phenomena.

The rest of the paper is organized as follows: Section 2 presents the econometric framework. In Section 2.1, we set out the dynamic conditional framework, while in Section 2.2, we discuss the process of rank transformation and the rank-likelihood in a Bayesian framework. Section 2.3 describes how we implement Gibbs sampling to estimate a sparse, unconditional precision matrix. Section 3 describes the estimation of the Bayesian nonparanormal dynamic conditional partial correlation alongside a GARCH(1,1) model. Section 3.1 addresses the Bayesian estimation procedure for the GARCH(1,1) model, while Section 3.2 outlines a specific algorithm for computing the posterior distribution. Section 4 details the MC simulation designs and provides a summary of the main findings for the proposed Bayesian estimators. In Section 5, we apply our estimation framework to two sets of empirical data: daily foreign stock price indices (presented in Section 5.1) and daily returns on securities selected from S&P 500 (presented in Section 5.2). Section 6 summarizes the research and its implications. Supplementary material, including technical specifics and additional empirical visualizations, is presented in the appendix.

2 Bayesian Nonparanormal Dynamic Conditional Model

2.1 Dynamic conditional framework

Let y_{it} be the return of financial security i at time t, comprised of the rate of price change plus dividends if applicable. Define $\mathbf{y}_t = (y_{1t}, y_{2t}, \ldots, y_{Nt})'$ as the vector of returns for N securities at time t, and $\mathcal{F}_t$ as the information set available up to time t for $t = 1, 2, \ldots, T$. The return process is modeled as follows:

$$\mathbf{y}_t = \boldsymbol{\mu}_t + \boldsymbol{\Sigma}_t^{1/2} \boldsymbol{\epsilon}_t, \quad \text{for } t = 1, 2, \ldots, T, \tag{2.1}$$

where $\boldsymbol{\mu}_t = \mathbb{E}(\boldsymbol{y}_t|\mathcal{F}_{t-1}) = (\mu_{1t}, \mu_{2t}, \ldots, \mu_{Nt})$ is the conditional mean vector, and $\boldsymbol{\Sigma}_t = \{\sigma_{ij,t}\}_{i,j=1}^{N} = \text{Cov}\,(\mathbf{y}_t|\mathcal{F}_{t-1})$ represents the $N \times N$ positive-definite conditional covariance matrix. The error vectors $\boldsymbol{\epsilon}_t$ are assumed to be *i.i.d.* with $\mathbb{E}(\boldsymbol{\epsilon}_t|\mathcal{F}_{t-1}) = 0$ and $\mathbb{E}(\boldsymbol{\epsilon}_t\boldsymbol{\epsilon}_t'|\mathcal{F}_{t-1}) = \mathbb{I}_N$, where $\mathbb{I}_N$ is the identity matrix of order N.

Following the literature, $\boldsymbol{\Sigma}_t$ is expressed as

$$\boldsymbol{\Sigma}_t = \mathbf{D}_t^{1/2}\mathbf{R}_t\mathbf{D}_t^{1/2}, \tag{2.2}$$

where $\mathbf{D}_t^{1/2} = \text{diag}\{\boldsymbol{\Sigma}_t^{1/2}\} = \text{diag}\{\sigma_{11,t}^{1/2}, \ldots, \sigma_{NN,t}^{1/2}\}$ contains the conditional standard deviations, $\mathbf{R}_t = \mathbf{S}_t^{-1}$, and $\mathbf{S}_t$ is the conditional inverse correlation matrix. Conditional variances, $\sigma_{ii,t}$, is assumed to follow GARCH(1,1) processes:

$$\sigma_{ii,t} = \mathrm{a}_i + \theta_{0i}r_{i,t-1}^2 + \theta_{1i}\sigma_{ii,t-1}, \tag{2.3}$$

with parameters $(\mathrm{a}_i, \theta_{0i}, \theta_{1i})$, where $\mathrm{a}_i > 0$, $\theta_{0i} \geq 0$, $\theta_{1i} \geq 0$, $\theta_{0i} + \theta_{1i} < 1$ for $i = 1, 2, \ldots, N$, and $r_{it} = y_{it} - \mu_t$.[2]

Remark 1. The GARCH(1,1) specification in (2.3), requires positive parameters to ensure positive conditional variance and incorporates short memory and symmetric volatility reactions. We address the model's tendency towards skewness and heavy tails in the error distribution through a Bayesian estimation approach, utilizing a multivariate t-distribution with ν degrees of freedom as suggested by Fioruci, Ehlers, and Andrade Filho (2014). While aware of alternative GARCH variants such as exponential GARCH (EGARCH; Nelson 1991), quadratic GARCH (QGARCH; Sentana 1995), threshold GARCH (Chen and So, 2006; Chen, Liu, and So, 2008), and fractionally integrated GARCH (FIGARCH; Baillie, Bollerslev, and Mikkelsen 1996) that might mitigate the GARCH(1,1) model's limitations, our methodological choice remains justified by our primary analytical focus.

Our primary focus is on estimating the conditional precision matrices, $\mathbf{P}_t$, and the conditional inverse correlation matrices, $\mathbf{S}_t$, instead of deriving the conditional covariance and conditional correlation, $\mathbf{R}_t = \mathbf{S}_t^{-1}$, matrices from $\boldsymbol{\Psi}_t$. The conditional partial correlation matrix, $\boldsymbol{\Psi}_t$ is also of special interest as they provide a model of appropriate measure of pair-wise conditional dependence, which is derived as $\psi_{ij,t} = -s_{ij,t}$, $i \neq j$. Contrary to the conventional application of the DCC procedure to the conditional covariance matrix, applying the procedure to the conditional precision matrix has the added advantage of bypassing the inversion of the estimated inverse conditional covariance matrix, thereby facilitating portfolio optimization and the validation of asset pricing theory.

[2]The restriction $\mathrm{a}_i > 0$ is required for our analysis due to the use of Bayesian GARCH(1,1) estimation, where a_i is sampled from a normal distribution in our estimation process. This contrasts with the standard GARCH(1,1) process, where the restriction is unnecessary owing to the steady-state condition, $\mathrm{a}_i = \sigma_{i0}(1 - \theta_{0i} - \theta_{1i})$, where σ_{i0} is the long-term variance.

The standard DCC–MGARCH model (Engle, 2002), as specified in Equations (2.1)–(2.3) using $\mathbf{S}_t^{-1} = \mathbf{R}_t$ is defined as

$$\mathbf{R}_t = \text{diag}\{\mathbf{Q}_t\}^{-1/2}\mathbf{Q}_t\text{diag}\{\mathbf{Q}_t\}^{-1/2},$$

where $\mathbf{Q}_t$ is an $N \times N$ symmetric positive-definite matrices defined by,

$$\mathbf{Q}_t = (1 - a - b)\boldsymbol{\Sigma} + a\mathbf{u}_{t-1}\mathbf{u}_{t-1}' + b\mathbf{Q}_{t-1}, \tag{2.4}$$

$\mathbf{u}_t = \mathbf{D}_t^{-1}(\mathbf{y}_t - \boldsymbol{\mu}_t)$, $\boldsymbol{\Sigma}$ is the unconditional covariance matrix of $\mathbf{u}_t$, $a > 0$, $b > 0$ and $a + b < 1$. However, applying this framework to the precision matrix leads to complications, as the matrix $\mathbf{u}_{t-1}\mathbf{u}_{t-1}'$ is at most semi-positive definite and thus non-invertible. A varying correlation MGARCH (VC–MGARCH) model (Tse and Tsui, 2002) circumvents this issue by estimating conditional correlations, substituting $\mathbf{u}_{t-1}\mathbf{u}_{t-1}'$ with the sample correlation matrix over $(\mathbf{u}_{t-1}, \ldots, \mathbf{u}_{t-M})$, where $M \geq N$. Similarly, the dynamic correlation MSV (DC–MSV) model (Asai and McAleer, 2009) employs a Wishart process as an alternative to $\mathbf{u}_{t-1}\mathbf{u}_{t-1}'$ while maintaining the standard model's conditional covariance matrices.

Billio, Caporin, and Gobbo (2003) propose a block-diagonal structure to restrict the dynamic to be equal only among groups of variables. As an extension, the clustered correlation MGARCH model (CC-MGARCH) proposed by So and Yip (2012) integrates these group-specific effects into the estimation of the direct conditional correlation matrix, where a Bayesian model selection selects the cluster. Although this adjustment increases the model's flexibility to capture various dependencies, it also significantly increases the number of unknown parameters when combined with the conditional variance structure outlined in Equation (2.3). Such complexity present new challenges for estimation methodologies and complicates interpretations, particularly for large-dimensional datasets. In these large-dimensional cases, Engle, Ledoit, and Wolf (2019) and De Nard, Ledoit, and Wolf (2021) follow the same framework as presented in (2.4) incorporating regularization techniques only for estimation of unconditional covariance matrix $\boldsymbol{\Sigma}$ using shrinkage methods.

In our approach, we consider directly the conditional inverse correlation matrix, $\mathbf{S}_t = \{s_{ij,t}\}$, in (2.2), and set

$$\mathbf{S}_t = \text{diag}\{\mathbf{P}_t\}^{-1/2}\mathbf{P}_t\text{diag}\{\mathbf{P}_t\}^{-1/2}, \tag{2.5}$$

where $\mathbf{P}_t$ represents $N \times N$ symmetric positive-definite conditional precision matrices given by

$$\mathbf{P}_t = (1 - a - b)\,\boldsymbol{\Omega} + a\boldsymbol{\Xi}_{t-1} + b\mathbf{P}_{t-1}, \tag{2.6}$$

with the corresponding parameters $a > 0$, $b > 0$ and $a + b < 1$. As noted above, we estimate the conditional precision matrix by using the precision matrix of the lagged residual, $\boldsymbol{\Xi}_{t-1}$, to avoid

the issue of non-invertibility. Furthermore, we incorporate a shrinkage prior in the sampling process of the unconditional precision matrix, $\mathbf{\Omega}$.

To obtain $\mathbf{\Omega}$, we begin with the transformation of raw devolatilized residuals, $\mathbf{u}_t = \mathbf{D}_t^{-1}(\mathbf{y}_t - \boldsymbol{\mu}_t)$, aiming to approximate a multivariate Gaussian distribution. This transformation, facilitated by the Nonparanormal rank transformation detailed in Section 2.2 below, converts the raw devolatilized residual matrix $\mathbf{U} = (\mathbf{u}_1, \mathbf{u}_2, \ldots, \mathbf{u}_T)'$ into a rank transformed devolatilized residual matrix $\mathbf{Z} = (\mathbf{z}_1, \mathbf{z}_2, \ldots, \mathbf{z}_T)'$ following the multivariate normal distribution with $\mathbf{0}$ mean and the correlation matrix $\mathbf{C}$ which has an inverse correlation matrix $\mathbf{C}^{-1} = \text{diag}\{\mathbf{\Omega}\}^{-1/2}\mathbf{\Omega}\text{diag}\{\mathbf{\Omega}\}^{-1/2}$. The objective of this transformation is to achieve approximated Gaussian standardized residuals, thereby imbuing the resultant partial correlation matrices with meaningful interpretability concerning conditional dependence—one of the focal points of our exploration into volatility dependence in this paper. Then, the unconditional precision matrix, $\mathbf{\Omega}$, is sampled from the posterior distribution regularized with horseshoe priors using Gibbs sampling, as elaborated in Section 2.3 below.

We obtain the lagged residual precision matrix $\mathbf{\Xi}_{t-1}$, in (2.6) by drawing samples from a conjugate posterior distribution following a Wishart distribution:

$$\mathbf{\Xi}_{t-1} \sim \mathcal{W}\left(T+3, (\mathbb{I}_N + \mathbf{z}_{t-1}\mathbf{z}_{t-1}')^{-1}\right), \tag{2.7}$$

where $T+3$ is the degrees of freedom, and $(\mathbb{I}_N+\mathbf{z}_{t-1}\mathbf{z}_{t-1}')^{-1}$ is the scale matrix. This distribution is particularly suited for our purposes as it ensures that the sampled precision matrices are symmetric and positive-definite. The conjugacy with the approximated normal distribution of $\mathbf{z}_t$, as made possible by the nonparanormal transformation, permits closed-form expressions for the posterior. The Wishart distribution, a probability distribution over symmetric positive-definite matrices, inherently captures the structure and dependencies in the data. We, therefore, sample the conditional precision matrix for the conditional covariance structure of the rank-transformed residuals, $\mathbf{z}_{t-1}$. This matrix reflects the dynamic volatility and interrelationships among $\mathbf{z}_{t-1}$ variables. The inclusion of $\mathbb{I}_N$ in the scale matrix in (2.7) ensures its positive definiteness and invertibility, serving as regularization to prevent overfitting by limiting excessive adaptation to recent observations. It also establishes a baseline assumption of independent variables with unit variance.

Building upon this framework, we can define the conditional partial correlation matrix $\mathbf{\Psi}_t = \{\psi_{ij,t}\}_{i,j=1}^N$, which is closely linked to $\mathbf{S}_t$, by setting $\psi_{ij,t}$ as follows:

$$\psi_{ij,t} = \begin{cases} -s_{ij,t}/\sqrt{s_{ii,t}s_{jj,t}}, & \text{for } i \neq j \\ 1 & \text{for } i = j \end{cases}. \tag{2.8}$$

Through the application of the nonparanormal rank transformation, one can interpret the el-

ements of $\mathbf{\Psi}_t$ as indicators of conditional dependence. This transformation assures the adaptability of the standard Gaussian-based interpretation of partial correlations to our framework, hence allowing the inference of conditional dependence from the observed data.

Remark 2. If the devolatilized residuals do not follow a multivariate normal distribution, the partial correlations cannot be straightforwardly interpreted as measures of conditional dependence due to the potential nonlinearity and skewness in the relationships between variables. The Gaussian assumption ensures that the partial correlations describe linear relationships and that the measure of zero partial correlation corresponds to conditional dependence. In the absence of multivariate normality, reliance on partial correlations for such interpretations necessitates prudence. Alternative analytical strategies, such as the employment of copula models or the adoption of nonparametric measures like distance correlation and mutual information, may be necessary to attain robust inference.

2.2 Bayesian rank transformation and likelihood

To infer the unconditional precision matrix $\mathbf{\Omega}$, we transform the raw devolatilized residuals $\mathbf{U} = (\mathbf{u}_1, \mathbf{u}_2, \ldots, \mathbf{u}_T)' = (\mathbf{U}_1, \mathbf{U}_2, \ldots, \mathbf{U}_N)$ into the rank transformed devolatilized residuals $\mathbf{Z} = (\mathbf{z}_1, \mathbf{z}_2, \ldots, \mathbf{z}_T)' = (\mathbf{Z}_1, \mathbf{Z}_2, \ldots, \mathbf{Z}_N) \sim \mathcal{N}(\mathbf{0}, \mathbf{C})$, where $\mathbf{C} = \mathbf{S}^{-1}$. We delineate the set $\mathcal{B} = \{\mathbf{Z} \in \mathbb{R}^{T \times N} : u_{i,t_{r-1}} < u_{i,t_r} < u_{i,t_{r+1}}\}$, given the monotone and increasing transformation functions g_i, such that $i = 1, 2, \ldots, N$, and $t = 1, 2, \ldots, T$ with a rank of the observations $r = 2, 3, \ldots, T-1$. The rank-transformed residuals $\mathbf{Z}$ are restricted to reside within this set. Utilizing Gibbs sampling as described in Algorithm 2, Appendix A, we can obtain $\mathbf{Z}$.

The rank-likelihood $L^{\mathrm{RL}}(\mathbf{Z})$ is then given by

$$L^{\mathrm{RL}}(\mathbf{Z}) = \Pr(\mathbf{Z} \in \mathcal{B} | \mathbf{C}, g_1, g_2 \ldots, g_N) = \int_{\mathcal{B}} p(\mathbf{Z}|\mathbf{C})\, d\mathbf{Z} = \Pr(\mathbf{Z} \in \mathcal{B}|\mathbf{C}), \tag{2.9}$$

where $g_1, g_2 \ldots, g_N$ are transformation functions. This likelihood is exclusively contingent on $\mathbf{C}$ and is devoid of dependency on specific transformation functions (Hoff, 2007).

Example 1. (Hoff, 2007) Suppose we are interested in estimating the parameter θ but there is also a nuisance parameter g that we are not interested in. We find a statistic $z = t(u)$ which is a function of our observed data u, where the distribution of $t(u)$ depends only on θ and is independent of the nuisance parameter g. Then, we can have the relationship as follows:

$$p(u|\theta, g) = p(t(u), u|\theta, g) = p(t(u)|\theta) \cdot p(u|t(u), \theta, g).$$

This expression implies that the probability distribution of observed data u, given both θ and g, can be decomposed as the distribution of the statistic $t(u)$ and the distribution of u, given $t(u)$,

θ, and g. Since $t(u)$ is independent of g, we can focus on $p(t(u)|\theta)$ for estimating θ, ignoring the nuisance parameter g in the estimation process.

To achieve (2.9), we can rewrite $\mathbf{Z}$ as $(\mathbf{Z}_1, \mathbf{Z}_2, \ldots, \mathbf{Z}_N) = (g_1(\mathbf{U}_1), g_2(\mathbf{U}_2), \ldots, g_N(\mathbf{U}_N)) \sim \mathcal{N}(\mathbf{0}, \mathbf{C})$. Then, since $\mathbf{Z} \in \mathcal{B}$ occurs whenever $\mathbf{U}$ is observed, the raw devolatilized residuals likelihood of $\mathbf{U}$ is

$$\begin{aligned} p(\mathbf{U}|\mathbf{C}, g_1, g_2, \ldots, g_N) &= p\left(\mathbf{Z} \in \mathcal{B}, \mathbf{U}|\mathbf{C}, g_1, g_2, \ldots, g_N\right) \\ &= \Pr(\mathbf{Z} \in \mathcal{B}|\mathbf{C}) \cdot p(\mathbf{U}|\mathbf{Z} \in \mathcal{B}, \mathbf{C}, g_1, g_2, \ldots, g_N). \end{aligned}$$

Therefore, $\Pr(\mathbf{Z} \in \mathcal{B}|\mathbf{C})$ alone can be used to estimate $\mathbf{C}$, as it is dependent only on the parameter of interest, $\mathbf{C}$, rather than the transformation functions, $g_1, g_2, \ldots, g_N$. Then, using the reparameterization in terms of the non-identifiable $\mathbf{\Omega}$, but focusing on the identifiable unconditional inverse correlation matrix, $\mathbf{S}$, we can derive the posterior distribution

$$\Pr(\mathbf{S}|\mathbf{Z} \in \mathcal{B}) \propto p(\mathbf{S}) p(\mathbf{Z} \in \mathcal{B}|\mathbf{S}). \tag{2.10}$$

This rank-based nonparanormal approach deviates from both the Copula and the standard nonparanormal frameworks by simplifying the overall modeling process. The Copula model mandates a two-step transformations. Initially, $\mathbf{U}_i$, for $i = 1, 2, \ldots, N$ are transformed into the uniform margins $\tilde{\mathbf{U}}_i$ via their respective empirical cumulative distribution functions (CDFs), $\tilde{\mathbf{U}}_i = F_i(\mathbf{U}_i) \sim \mathcal{U}(0, 1)$ for $i = 1, 2, \ldots, N$. Subsequently, these uniform variables are converted back to standard normal margins by employing the inverse standard normal CDF, Φ^{-1}, denoted as $\mathbf{Z}_i = \Phi^{-1}(\tilde{\mathbf{U}}_i)$. The joint likelihood $L^{\mathrm{CP}}(\mathbf{Z})$ in the Gaussian copula model is then constructed as the product of individual marginal likelihoods and the copula density, represented as

$$L^{\mathrm{CP}}\left(\mathbf{Z}\right) = \prod_{i=1}^{N} f\left(\mathbf{Z}_i\right) \cdot c\left(\mathbf{Z}; \mathbf{C}\right), \tag{2.11}$$

where $f(\mathbf{Z}_i)$ is the marginal density of $\mathbf{Z}_i$, $c(\mathbf{Z}; \mathbf{C})$ denotes the copula density, and $\mathbf{C}$ is the correlation matrix capturing the dependencies among the $\mathbf{Z}_i$'s. The likelihood function in this approach decomposes into marginal and copula components. On the other hand, the standard nonparanormal model extends the Copula model's approach of formulating likelihood by introducing smooth, invertible functions to transform the original variables before the copula transformation, leading to a likelihood formulation that also involves these transformation functions g_i, resulting in transformed observations $g_i(u_{it})$. The core premise of the standard nonparanormal framework is that these transformed variables approximate a multivariate Gaussian distribution, obviating the need for additional transformations to uniform or standard normal margins. Under this Gaussian assumption, the joint likelihood $L^{\mathrm{NP}}(\mathbf{Z})$ for the transformed

dataset $\mathbf{Z}$, where $z_{it} = g_i(u_{it})$, is formulated as

$$L^{\mathrm{NP}}(\mathbf{Z}) = \prod_{i=1}^{N} \prod_{t=1}^{T} f(z_{it}) \cdot |J(g_i(u_{it}))|, \tag{2.12}$$

where $f(z_{it})$ denotes the Gaussian density function for the transformed variables z_{it} and $|J(g_i(u_{it}))|$ is the Jacobian determinant of the transformation g_i at u_{it}. This likelihood construction directly models the dependencies among variables and across time, capitalizing on the Gaussian approximation.

The rank-based nonparanormal model serves as an intermediary between the Copula and traditional nonparanormal frameworks. It avoids the Copula model's requisite partitioning of marginal and Copula components, thereby streamlining the likelihood formulation. Simultaneously, it circumvents the standard nonparanormal model's need for estimating smooth transformation functions g_i, thereby reducing model complexity. In short, this approach amalgamates the respective merits of both models while attenuating their individual complexities and assumptions.

We consider a new approach by integrating the DCC framework with the rank-based nonparanormal model, as proposed by Mulgrave and Ghosal (2023). We tackle the issue of non-identification in the rank-likelihood approach to derive the identifiable conditional precision matrix $\mathbf{P}_t = (p_{ij,t})$. This involves reparameterizing the model to use the non-identifiable $\mathbf{\Omega}$, and computing the non-identified conditional precision matrix $\tilde{\mathbf{P}}_t$ using Equation (2.6). We, then, focus on posterior inference for the identifiable conditional inverse correlation matrix $\mathbf{S}_t = (s_{ij,t})$, defined as $\mathbf{S}_t = \mathrm{diag}\{\tilde{\mathbf{P}}_t\}^{-1/2}\tilde{\mathbf{P}}_t\mathrm{diag}\{\tilde{\mathbf{P}}_t\}^{-1/2}$. Since the rank-likelihood is unaffected by scale transformations, both non-identifiable and identifiable models produce the same posterior distributions, as indicated in Equation (2.10). This allows us to sample from the posterior distribution of $\mathbf{S}_t$ without the need to estimate transformation functions. Given $\mathbf{S}_t$, we can obtain the conditional variance $\sigma_{ii,t}$ by employing a GARCH(1,1) process for each security. Therefore, we can find the identifiable conditional precision matrix $\mathbf{P}_t$, where

$$p_{ij,t} = s_{ij,t}\sqrt{(1/\sigma_{ii,t})(1/\sigma_{jj,t})} \tag{2.13}$$

under the Gaussian distribution (Rue and Held, 2005, p.26).

2.3 Using Gibbs sampling to obtain the unconditional precision matrix

We obtain the unconditional precision matrix $\mathbf{\Omega}$ by sampling the Cholesky decomposition $\mathbf{\Omega} = \mathbf{L}\mathbf{L}'$, where $\mathbf{L}$ is a lower triangular matrix. The lower triangular elements of $\mathbf{\Omega}$ are defined as $\Omega_{ij} = \sum_{k=1}^{j} L_{ik}L_{jk}$ for $j = 1, 2, \ldots, N$ and $i = j+1, j+2, \ldots, N$. The elements of $\mathbf{L}$ are determined such that:

$$L_{ij} = \begin{cases} \sqrt{\Omega_{ii} - \sum_{k=1}^{i-1} L_{ik}^2}, & \text{if } i = j, \\ \frac{1}{L_{jj}} \left(\Omega_{ij} - \sum_{k=1}^{j-1} L_{ik} L_{jk} \right), & \text{if } i > j, \\ 0, & \text{if } i < j. \end{cases}$$

Then, the density of $\mathbf{Z} \sim \mathcal{N}(\mathbf{0}, \mathbf{\Sigma})$ is

$$p(\mathbf{Z}) = (2\pi)^{-\frac{N}{2}} |\mathbf{\Omega}|^{\frac{1}{2}} \exp\left(-\frac{1}{2} \mathbf{Z}' \mathbf{\Omega} \mathbf{Z} \right)$$

and the conditional distribution of $\mathbf{Z}_j$ given $\mathbf{Z}_{i>j}$ is Gaussian, with the mean and variance derived from the elements of $\mathbf{L}$: for $j = 1, 2, \ldots, N$,

$$\mathbf{Z}_j | \mathbf{Z}_{i>j} \sim \mathcal{N}\left(\sum_{i=1}^{j-1} -\frac{L_{ij}}{L_{jj}} \mathbf{Z}_i, \frac{1}{L_{jj}^2} \right),$$

where $-L_{ij}/L_{jj}$ represents the regression coefficient of $\mathbf{Z}_j$ on $\mathbf{Z}_i$, and $1/L_{jj}^2$ is the conditional variance. Therefore, we can represent the Cholesky decomposition with the regression coefficient,

$$\Omega_{ij} = \sum_{k=1}^{j} L_{ik} L_{jk} = \sum_{k=1}^{j} \beta_{ik} \beta_{jk} \omega_k, \tag{2.14}$$

where $\beta_{ij} = -L_{ij}/L_{jj}$ represents the regression coefficients, and $\omega_j = 1/\sigma_j^2 = L_{jj}^2$ denotes the precision of the multivariate Gaussian distribution. Using (2.14), we can formulate the regression problem (Rue and Held, 2005, p. 35). By employing the rank transformed devolatilized residuals $\mathbf{Z} \sim \mathcal{N}(\mathbf{0}, \mathbf{\Sigma})$, where $\mathbf{\Sigma}$ is the unconditional covariance matrix, we can have

$$\mathbf{Z}_j = \sum_{i>j} \beta_{ij} \mathbf{Z}_i + \eta_j, \quad \eta_j \sim \mathcal{N}\left(0, \omega_j^{-1}\right) \tag{2.15}$$

for $j = 1, 2, \ldots, N$ and $i = j+1, j+2, \ldots, N$. This formulation ensures the properties of symmetry and positive definiteness in the precision matrix. Based on Equation (2.15), the likelihood function takes the form

$$\mathbf{Z}_j | \mathbf{Z}_{i>j}, \boldsymbol{\beta}_{i>j}, \sigma_j^2 \sim \mathcal{N}\left(\mathbf{Z}_{i>j} \boldsymbol{\beta}_{i>j}, \sigma_j^2 \mathbb{I} \right), \tag{2.16}$$

where $\mathbf{Z}_{i>j}$ refers to the matrix constructed by the columns of $\mathbf{Z}$ greater than j, and $\boldsymbol{\beta}_{i>j} = (\beta_{j+1,j}, \beta_{j+2,j}, \ldots, \beta_{N,j})$.

In this regression model, there is an intrinsic sequence to the variables. To accommodate an order between variables, we impose a sparsity constraint on the rows of the lower triangular matrix, following the approach outlined by Mulgrave and Ghosal (2022). This method ensures

that the likelihood of non-zero elements remains uniform across rows, dictated by the ratio $\frac{c}{N\sqrt{i}}$, where c is an tuning parameter.[3] In this paper, we set $c = 0.1$ for all analyses to adapt to the high-dimension settings in the multivariate volatility model, thereby reducing the number of nonzero elements in each row of the unconditional precision matrix. For the regression coefficients β_{ij}, we employ a horseshoe prior, as delineated in Neville, Ormerod, and Wand (2014), with the global scale parameter $\tilde{\lambda}_j$ approximating the probability of a nonzero element. Characterized by its concentration around zero and tails resembling a Cauchy distribution, the horseshoe prior offers robust variable selection and the ability to capture extreme values. This selection stands in contrast to other commonly used priors such as the Gaussian and Laplace priors, which are limited by their lighter tails and less effective variable selection capabilities. The spike-and-slab prior, while designed to induce sparsity (Li and McCormick, 2019; Mulgrave and Ghosal, 2020) can be computationally demanding and less apt at modeling heavy-tailed features. The G-Wishart prior (Mohammadi and Wit, 2015; Mohammadi, Abegaz, Heuvel, and Wit, 2017), on the other hand, is tailored to capture structural sparsity in graph-based models but may not be optimal for handling heavy-tailed features. Hence, the horseshoe prior provides a balanced and effective choice for modeling the precision matrix's sparsity and tail behavior of the attributes that are frequently observed in financial data.

The combined application of sparsity constraints and carefully chosen priors induces a structured prior on $\mathbf{\Omega}$, subsequently influencing the prior on $\mathbf{S}$. For a comprehensive exposition of the sparsity mechanism, the reader references to Mulgrave and Ghosal (2022). The specific algorithm employed for the implementation is elaborated is given by Algorithm 3, in the Appendix A.

3 Bayesian nonparanormal dynamic conditional partial correlation – GARCH model estimation

Section 3.1 details the Bayesian GARCH(1,1) model's application within the DCC framework, emphasizing conditional variance calculation and the use of skewed distributions for modeling asymmetry and tail characteristics. Section 3.2 discusses the strategies for posterior computation, including optimization for initial parameters and an adaptive Metropolis-Hastings MCMC approach to address the computational challenges in large-dimensional settings.

[3]The Cholesky $\mathbf{L}$ of the unconditional precision matrix $\mathbf{\Omega}$ depends on the row index because $\Pr(\Omega_{ij} \neq 0) = \Pr(\sum_{k=1}^{N} l_{ik}l_{jk} \neq 0) = 1 - (1 - \rho_i\rho_j)^{\min(i,j)}$, where ρ_i is the probability of non-zero entry in the ith row of $\mathbf{L}$. Mulgrave and Ghosal (2022) set $\rho_i = c/(N\sqrt{i})$ to tune the sparsity constraint.

3.1 Bayesian GARCH(1,1) estimation

The conditional likelihood function, corresponding to Equation (2.1), is given by

$$
\begin{aligned}
l\left(\boldsymbol{\theta}|\mathbf{Y}\right) &= \prod_{t=1}^{T} \left|\boldsymbol{\Sigma}_t\right|^{-1/2} p_{\boldsymbol{\epsilon}}\left(\mathbf{P}_t^{-1/2}\mathbf{y}_t\right) \\
&= \prod_{t=1}^{T} \left[\prod_{i=1}^{N} \sigma_{ii,t}^{-1/2}\right] \left|\mathbf{S}_t^{-1}\right|^{-1/2} p_{\boldsymbol{\epsilon}}\left[\left(\mathbf{D}_t\mathbf{S}_t^{-1}\mathbf{D}_t\right)^{-1/2}\mathbf{y}_t\right],
\end{aligned}
$$

where $p_{\boldsymbol{\epsilon}}$ represents the joint density function of $\boldsymbol{\epsilon}_t$, parameterized by $\{\mathrm{a}_1, \theta_{10}, \theta_{11}, \ldots, \mathrm{a}_N, \theta_{N0}, \theta_{N1}, a, b\}$ in Equations (2.6) and (2.3). We adopt the multivariate skewed distributions characterized by a shape parameter $\gamma_i > 0$, which quantifies the degree of asymmetry as proposed by Bauwens and Laurent (2005):

$$
p_{\boldsymbol{\epsilon}}\left(\boldsymbol{\epsilon}_t|\boldsymbol{\gamma}\right) = 2^N \left(\prod_{i=1}^{N} \frac{\gamma_i \sigma_{\gamma_i}}{1+\gamma_i^2}\right) \frac{\Gamma\left((\nu+N)/2\right)}{\Gamma\left(\nu/2\right)\left[\pi(\nu-2)\right]^{N/2}} \left[1 + \frac{\boldsymbol{\epsilon}_t^{*\prime}\boldsymbol{\epsilon}_t^{*}}{\nu-2}\right]^{-\frac{\nu+N}{2}}, \tag{3.1}
$$

and

$$
\boldsymbol{\epsilon}_t^{*} = \begin{cases} (\boldsymbol{\epsilon}_t\sigma_{\gamma_i} + \mu_{\gamma_i})/\gamma_i & \text{if } \boldsymbol{\epsilon}_t \geq -\mu_{\gamma_i}/\sigma_{\gamma_i} \\ (\boldsymbol{\epsilon}_t\sigma_{\gamma_i} + \mu_{\gamma_i})\gamma_i & \text{if } \boldsymbol{\epsilon}_t < -\mu_{\gamma_i}/\sigma_{\gamma_i} \end{cases},
$$

where $\Gamma(\cdot)$ denotes the Gamma function, μ_{γ_i} and $\sigma_{\gamma_i}^2$ are defined by

$$
\begin{aligned}
\mu_{\gamma_i} &= \frac{\Gamma((\nu-1)/2)\sqrt{\nu-2}(\gamma-1/\gamma)}{\sqrt{\pi}\Gamma(\nu/2)}, \\
\sigma_{\gamma_i}^2 &= (\gamma_i^2 + 1/\gamma_i^2) - \mu_{\gamma_i}^2 - 1,
\end{aligned}
$$

and ν is the degree of freedom to (tail) parameter. This methodology decouples the influence of skewness and tail characteristics while anchoring the mode at zero. The shape parameter, γ_i, governs the distribution of mass on either side of the mode, whereas the tail parameter, ν, modulates the distribution's skewness. $\gamma_i = 1$ yields symmetric distributions, while $\gamma_i > 1$ and $\gamma_i < 1$give right and left skewness, respectively. As $\nu \to \infty$, the distribution converges to a standard multivariate normal distribution, as demonstrated by Fernández and Steel (1998).

For the GARCH(1,1) coefficients in Equation (2.3), we follow the prior distributions pro-

posed by Ardia (2008), for $i = 1, 2, \ldots, N$,

$$\begin{aligned}
\mathrm{a}_i &\sim \mathcal{N}\left(\mu_{\mathrm{a}_i}, \sigma^2_{\mathrm{a}_i}\right) I\left(\mathrm{a}_i > 0\right), \\
\theta_{0i} &\sim \mathcal{N}\left(\mu_{\theta_{0i}}, \sigma^2_{\theta_{0i}}\right) I\left(0 < \theta_{0i} < 1\right), \\
\theta_{1i} &\sim \mathcal{N}\left(\mu_{\theta_{1i}}, \sigma^2_{\theta_{1i}}\right) I\left(0 < \theta_{1i} < 1\right),
\end{aligned}$$

where $I(A)$ denotes an indicator function with $I(A) = 1$ if A holds and zero otherwise. Analogously, the priors for parameters a and b in Equation (2.6) are

$$a \sim \mathcal{N}\left(\mu_a, \sigma^2_a\right) I\left(0 < a < 1\right), \quad b \sim \mathcal{N}\left(\mu_b, \sigma^2_b\right) I\left(0 < b < 1\right).$$

For the skewness and tail parameters γ_i and ν, the priors are specified as:

$$\gamma_i \sim \mathcal{N}\left(\mu_{\gamma_i}, \sigma^2_{\gamma_i}\right) I\left(\gamma_i > 0\right), \quad \nu \sim \mathcal{N}\left(\mu_\nu, \sigma^2_\nu\right) I\left(\nu > 2\right).$$

3.2 Posterior computation

We generate random samples of $\Pr(\mathbf{S}_t|\mathbf{Z} \in \mathcal{D})$ by employing the following steps. To efficiently explore the parameter space, an optimization problem targeting the log-posterior distribution is initially solved to acquire starting parameters. If the resultant Hessian matrix is not positive-definite, an adaptive Metropolis-Hastings Markov Chain Monte Carlo (MH-MCMC) strategy is employed to construct the proposal distribution. The proposal distribution is a key component that suggests the next point in the parameter space to explore. We first run using an initial proposal distribution, a simple Gaussian with a predetermined covariance matrix. The results of this 'pilot run' are then used to update the proposal distribution in two ways: First, we recalculate the covariance matrix of the proposal distribution to align with the empirical covariance of the sampled points, thereby better reflecting the shape and orientation of the target distribution. In this step, we aim to adjust the acceptance rate between 15% and 50%. Second, by adjusting the step size (scale) of the proposal distribution, which is achieved by multiplying the empirical covariance with a parameter based on the acceptance rate. This adjustment aims to optimize the rate at which new proposals are accepted to go within a range of 20% to 50%. We implement an initial 'pilot run' for sample generation, followed by an adaptation phase during which the proposed distribution is refined based on the empirical covariance matrix of the observed samples. These adaptations made iteratively or after a set number of iterations, are designed to improve the exploration of the parameter space, ensuring more efficient and effective convergence to the target distribution. The adapted proposal distribution and step-size are then utilized in the main MCMC run, as detailed in Algorithm 1.

In large-dimensional settings where the number of variables exceeds 25, the computational

Algorithm 1 Bayesian nonparanormal dynamic conditional partial correlation– GARCH(1,1)

for 1=1:#Simulation **do**
  Choose initial parameter values $\Theta_0 = \mathrm{a}_1, \theta_{10}, \theta_{11}, \ldots, \mathrm{a}_N, \theta_{N0}, \theta_{N1}, a, b$ for the model
  Compute **Log-Rank Likelihood**:
  Compute raw devolatalized residuals $\mathbf{U}$.
  Compute rank transformed devolatalized residuals $\mathbf{Z}$ from Algorithm 2.
  Sample regularized unconditional precision matrix $\mathbf{\Omega}$ from Algorithm 3.
  Given $\mathbf{\Sigma}_1$ and $\mathbf{Q}_1$ based on $\mathbf{\Omega}$ at $t = 1$,
  for $t > 1$ **do**
    Sample $\mathbf{\Xi}_t \sim \mathcal{W}((\mathbb{I} + \mathbf{z}'_{t-1}\mathbf{z}_{t-1})^{-1}, 3 + T)$.
    Update $\mathbf{P}_t$: $\mathbf{P}_t = (1 - a - b)\mathbf{\Omega} + a\Xi_t + b\mathbf{P}_{t-1}$.
    Compute $\mathbf{S}_t = \mathbf{P}_t / \sqrt{\mathrm{diag}\{\mathbf{P}_t\}\mathrm{diag}\{\mathbf{P}_t\}'}$.
    Update diagonal elements of $\mathbf{\Sigma}_t$ as specified in (2.3).
    Save the current $\mathbf{S}_t$ for later use.
    Update log-rank likelihood based on the error distribution specified in (3.1).
  end for
  Compute log-posterior for $\mathbf{S}_t$ from the found log-rank likelihood and log priors for Θ_t as specified in Section 3.1.
  Compute log-posterior for Θ_t from the log-posterior for $\mathbf{S}_t$ and log-Jacobian for Θ_t.
  Given log-posterior, generate a new parameter set by pertrubing the current parameter set and decide whether to accept the new parameter set based on the Metropolis-Hastings criterion.
end for
Compute the conditional partial correlation matrix $\mathbf{\Psi}_t$ as Equation (2.8) and the conditional precision matrix $\mathbf{P}_t$ from the acquired MH-MCMC samples of $\mathbf{S}_t$.

burden of estimating more than 100 parameters becomes prohibitive. To ameliorate this, we adopt an approach akin to that delineated in Pakel, Shephard, Sheppard, and Engle (2021). Specifically, initial parameters are derived from optimizing univariate GARCH models for each variable rather than through a joint fit under the log-posterior distribution. Subsequent analysis focuses solely on parameters pertinent to conditional partial correlation matrices and associated error distributions. This strategy effectively minimizes the number of jointly estimated parameters and the requisite pilot simulations for establishing a viable proposal distribution. Nonetheless, adaptive phase introduces complexities stemming from the approximations inherent in the initial parameters. An alternative strategy for approximating the full posterior distribution involves Bayesian variational inference. This avenue is not explored in the present study because of the flexibility of the MCMC approach to resolve the model complexity. We leave this for future research.

4 Monte Carlo Experiments

In this section, we investigate the small sample performance by our proposed Bayesian non-paranormal conditional estimator through Monte Carlo simulations. More specifically, our objective is to empirically verify whether the estimation of the conditional precision and inverse correlation matrices surpasses the approach of inverting estimated conditional covariance and correlation matrices. Our approach is benchmarked against several shrinkage and Copula-based estimators commonly integrated within the DCC model. In this regard, we consider the DCC-L and DCC-NL estimators of Ledoit and Wolf (2004b); Pakel, Shephard, Sheppard, and Engle (2021) and Engle, Ledoit, and Wolf (2019), respectively, as well as Patton (2009)'s Gaussian Copula and t-Copula estimators. For each estimator, including our proposed approach, we fit univariate GARCH(1,1) models to normalize the return series for each $i = 1, 2, \ldots, N$.

We begin by generating $y_{it}^{(r)}$, for $r = 1, 2, \ldots, R$ replications, as

$$y_{it}^{(r)} = \mu_t^{(r)} + u_{it}^{(r)}, \quad \text{for} \quad i = 1, 2, \ldots, N; t = 1, 2, \ldots, T,$$

where $\mu_t^{(r)} \overset{i.i.d.}{\sim} \mathcal{U}(0.5, 1.5)$. The errors $u_{it}^{(r)}$ are generated as

$$u_{it}^{(r)} = \sqrt{h_{it}^{(r)}}\varepsilon_{it}^{(r)}, \quad \text{for} \quad i = 1, 2, \ldots, N; t = -50, -49, \ldots, -1, 0, 1, \ldots, T-1, T,$$

where $u_{i,-50}^{(r)} = \sqrt{h_{i,-50}^{(r)}}\varepsilon_{i,-50}^{(r)}$, and $h_{i,-50}^{(r)} = \sigma_i^{2,(r)} \overset{i.i.d.}{\sim} (\frac{1}{2} + \frac{\chi^2(2)}{4})$. We consider two different distributions for $\varepsilon_{it}^{(r)}$ following

$$\varepsilon_{it}^{(r)} \overset{i.i.d.}{\sim} \mathcal{N}(0, 1), \quad \text{and} \quad \varepsilon_{it}^{(r)} \overset{i.i.d.}{\sim} \text{scale} \cdot t(\nu = 3),$$

where $\text{scale} = \sqrt{\frac{\nu-2}{\nu}}$ and ν is a degree-of-freedom. Define $\mathbf{h}_t^{(r)}$ and $\mathbf{r}_t^{(r)}$ as

$$\mathbf{h}_t^{(r)} = (h_{1t}^{(r)}, h_{2t}^{(r)}, \ldots, h_{Nt}^{(r)})' \quad \text{and} \quad \mathbf{r}_t^{(r)} = (r_{1t}^{(r)}, r_{2t}^{(r)}, \ldots, r_{Nt}^{(r)})' = \mathbf{y}_t^{(r)} - \boldsymbol{\mu}_t^{(r)}.$$

The conditional variance $\mathbf{h}_t^{(r)}$ are generated as:

$$\mathbf{h}_t^{(r)} = \mathbf{W}^{(r)} + \boldsymbol{\Theta}_0^{(r)}\mathbf{r}_{t-1}^{2,(r)} + \boldsymbol{\Theta}_1^{(r)}\mathbf{h}_{t-1}^{(r)} > 0, \tag{4.1}$$

where $\mathbf{W}^{(r)} = (w_1^{(r)}, w_2^{(r)}, \ldots, w_N^{(r)})'$, $w_i^{(r)} = (1 - \theta_{i0}^{(r)} - \theta_{i1}^{(r)})\sigma_i^{2,(r)}$, $\boldsymbol{\Theta}_0^{(r)} = \text{diag}\{\theta_{10}^{(r)}, \theta_{20}^{(r)}, \cdots, \theta_{N0}^{(r)}\}$ and $\boldsymbol{\Theta}_1^{(r)} = \text{diag}\{\theta_{11}^{(r)}, \theta_{21}^{(r)}, \cdots, \theta_{N1}^{(r)}\}$. The parameters are sampled from $\theta_{i0}^{(r)} \overset{i.i.d.}{\sim} \mathcal{U}(0.1, 0.2)$, $\theta_{i1}^{(r)} \overset{i.i.d.}{\sim} \mathcal{U}(0.5, 0.75)$, and $\sigma_i^{2,(r)} \overset{i.i.d.}{\sim} \left(\frac{1}{2} + \frac{\chi^2(2)}{4}\right)$, respectively. $\mathbf{y}_t^{(r)}$ are generated as:

$$\mathbf{y}_t^{(r)} = \boldsymbol{\mu}_t^{(r)} + \left\{\mathbf{D}_t^{(r)}\right\}^{1/2}\mathbf{L}_{\mathbf{S},t}^{-1}\boldsymbol{\varepsilon}_t^{(r)},$$

where $\mathbf{L}_{\mathbf{S},t}$ is a Cholesky factor of the conditional inverse correlation matrix

$$\mathbf{S}_t^{(r)} = \text{diag}\{\mathbf{P}_t^{(r)}\}^{-1/2}\mathbf{P}_t^{(r)}\text{diag}\{\mathbf{P}_t^{(r)}\}^{-1/2},$$

and $\mathbf{P}_t^{(r)}$ denotes a conditional precision matrix generated by simulation designs A and B below.

We focus on the problem of estimating both the conditional precision matrix, $\mathbf{P}_t$, and the conditional inverse correlation matrix, $\mathbf{S}_t$, for two particular cases of dense conditional precision matrices.

Monte Carlo design A: We consider a conditional precision matrix $\mathbf{P}_t^{(r)}$, which is structured such that 20% of its eigenvalues are 1, 40% are 1/3, and the remaining 40% are 1/10. This particular composition of the precision matrix is reflected in its associated covariance matrix $\mathbf{\Sigma}_t^{(r)}$, aligning with the eigenvalue distribution specified by Ledoit and Wolf (2012)—where 20% of the eigenvalues are 1, 40% are 3, and the remaining 40% are 10. For each time point $t = -50, -49, \ldots, -1, 0, 1, \ldots, T-1, T$, we proceed by creating a dense lower triangular Cholesky factor $\mathbf{L}_{\mathbf{P},t}^{(r)}$ of $\mathbf{P}_t^{(r)}$, with off-diagonal elements $L_{ij,t}^{(r)} \overset{i.i.d.}{\sim} \mathcal{N}(0,1)$ for $i > j$ and $L_{ii,t}^{(r)} \overset{i.i.d.}{\sim} \mathcal{N}(0, 0.1)$ for $i = 1, 2, \ldots, N$. We generate a diagonal matrix of eigenvalues $\mathbf{\Lambda}_t^{(r)} = \text{diag}\{\lambda_{1t}\boldsymbol{\tau}_1, \lambda_{2t}\boldsymbol{\tau}_2, \lambda_{3t}\boldsymbol{\tau}_3\}$, where $\boldsymbol{\tau}_1 = \mathbf{1}_{\lceil 0.2N \rceil}$ is a vector of ones with a length that comprises 20% of N, rounded up; $\boldsymbol{\tau}_2 = \mathbf{1}_{\lceil 0.4N \rceil}$ is a vector of ones representing 40% of N, also rounded up; and $\boldsymbol{\tau}_3 = \mathbf{1}_{N-\lceil 0.2N \rceil - \lceil 0.4N \rceil}$ is a vector of the remaining proportion of N. The eigenvalues are set at $\lambda_{1t} = 1$, $\lambda_{2t} = 1/3$, and $\lambda_{3t} = 1/10$. Finally, the conditional precision matrix $\mathbf{P}_t^{(r)}$ is constructed as

$$\mathbf{P}_t^{(r)} = \mathbf{L}_{\mathbf{P},t}^{(r)}\mathbf{\Lambda}_t^{(r)}\mathbf{L}_{\mathbf{P},t}^{(r)\prime}.$$

Monte Carlo design B: We generate a conditional precision matrix $\mathbf{P}_t^{(r)}$ with an underlying sparsity pattern for each time point $t = -50, -49, \ldots - 1, 0, 1, \ldots, T-1, T$. We first obtain a dense Cholesky factor $\mathbf{L}_t^{\text{dense},(r)} = (l_{ij,t}^{\text{dense},(r)})$ following Monte Carlo design A. First, we generate a binary selection matrix $\mathbf{M}_t^{\text{lower},(r)} = (m_{ij,t}^{\text{lower},(r)}) \overset{i.i.d.}{\sim} \text{Binomial}(1, 1-\kappa)$ for $i > j$, with κ determining the sparsity level. Subsequently, we construct a sparse Cholesky factor $\mathbf{L}_t^{\text{sparse},(r)} = (l_{ij,t}^{\text{sparse},(r)})$ through element-wise multiplication with the binary selection matrix: $l_{ij,t}^{\text{sparse},(r)} = l_{ij,t}^{\text{dense},(r)} \cdot m_{ij,t}^{\text{lower},(r)}$. The precision matrix $\mathbf{P}_t^{(r)}$ is then formed by

$$\mathbf{P}_t^{(r)} = \mathbf{L}_{\text{sparse},t}^{(r)}\mathbf{L}_{\text{sparse},t}^{(r)\prime} + \delta\mathbf{\Lambda}_t^{(r)},$$

where $\mathbf{\Lambda}_t^{(r)}$ is drawn from a Wishart distribution with $T+3$ degrees of freedom and the scale matrix $\mathbb{I}_N$; $\mathbf{\Lambda}_t^{(r)} \overset{i.i.d.}{\sim} \mathcal{W}(T+3, \mathbb{I}_N)$. The Wishart distribution, a multivariate extension of the chi-squared distribution, is conventionally employed for modeling the precision matrices of multivariate normal distributions. Opting for $T+3$ degrees of freedom results in reduced variability around the scale matrix $\mathbb{I}_N$, thereby conferring greater stability, albeit with potential amplifi-

cation, to the diagonal elements of the precision matrix $\mathbf{P}_t^{(r)}$ due to the additive term $\delta\mathbf{\Lambda}_t^{(r)}$. The selection of $\mathbb{I}_N$ as the scale matrix normalizes the expected conditional precision structure to be $(T+3)\mathbb{I}_N$ and establishes a quasi-orthogonal structure in $\mathbf{P}_t^{(r)}$. This choice perserves the structure of the sparse components, $\mathbf{L}_{\text{sparse},t}^{(r)}\mathbf{L}_{\text{sparse},t}^{(r)\prime}$, even when the sampled $\mathbf{\Lambda}_t$ predominates over them. $\delta\mathbf{\Lambda}_t$ introduces a dense components into $\mathbf{P}_t^{(r)}$, resulting a heterogeneous matrix with both sparse and dense parts. The parameter $\delta = 0.1$ regulates the magnitude of the dense components, ensuring that the noise they generate does not significantly alter the structure.

Remark 3. The construction of $\mathbf{P}_t^{(r)}$ in Monte Carlo design A requires further clarification, as it is not a sparse precision matrix. Instead, sparsity is imposed solely on its first term. The second term introduces denseness into the matrix, which is regulated by the parameter δ. This hybrid structure is motivated by extant literature that questions the empirical validity of sparsity assumptions, particularly in economics and finance. For instance, Giannone, Lenza, and Primiceri (2021) scrutinized multiple economic datasets and concluded that sparsity is generally not an inherent feature. Echoing this, they advocate for sparsity only when there is compelling evidence in advance supporting predictive models with a restricted set of explanatory variables (Barigozzi and Brownlees, 2019). Consequently, our simulation design incorporates both sparse and dense elements in $\mathbf{P}_t^{(r)}$ to more closely mimic the characteristics of real-world datasets. However, the incorporation of sparsity remains methodologically advantageous for computational tractability and interpretability. Additionally, sparse representations can offer a parsimonious yet effective approximation to complex, high-dimensional data structures.

Remark 4. In the first simulation design, the covariance matrix is highly unstable, yet the precision matrix exhibits a stable eigenvalue distribution. This situation often arises in high-dimensional settings where the number of variables significantly exceeds the sample size. While the covariance matrix becomes ill-conditioned or even singular due to this dimensionality issue, the corresponding precision matrix maintains stability in its eigenvalues. This phenomenon is relevant in covariance matrix estimation literature, where the primary focus is stabilizing the covariance matrix in high-dimensional data. Examples of such datasets include financial asset returns. On the other hand, the second simulation design considers the situation where, despite applying techniques to stabilize the covariance matrix, the precision matrix still can have an unstable eigenvalue distribution. This instability can occur due to factors intrinsic to the data, such as nonlinear relationships between variables, high noise levels, or outliers. These factors can distort the precision matrix, making it difficult to achieve stability through standard regularization or shrinkage methods. Examining these two designs, we aim to assess the resilience and accuracy of various estimation methods under different stability regimes.

4.1 Simulation Results

Our simulation presents results for different dimensions, $N \in \{25, 50, 100, 125\}$, and times, $T \in \{50, 100, 150, 200, 250\}$. We conducted $R = 100$ replications across these varying dimensions and periods. For our proposed Bayesian nonparanormal conditional estimation method, we perform $4,000$ iterations, with the first $2,000$ serving as the burn-in periods. When applying the Gibbs sampling algorithm, we fix the parameter c at 0.1 to induce substantial sparsity within the model. Concerning Bayesian GARCH parameters, we set all mean values to zero, $(\mu_{\omega_i} = \mu_{\theta_{0i}} = \mu_{\theta_{1i}} = \mu_a = \mu_b = \mu_{\gamma_i} = \mu_\nu = 0)$. We assign a value of 100 to all variance parameters, except for $\sigma^2_{\gamma_i}, i.e., \sigma^2_{\omega_i} = \sigma^2_{\theta_{0i}} = \sigma^2_{\theta_{1i}} = \sigma^2_a = \sigma^2_b = \sigma^2_\nu = 100$. For $\sigma^2_{\gamma_i}$, we selected 0.64^{-1} to obtain a variance for γ_i of approximately 0.57 and a probability of γ_i being between 0 and 1 of roughly 0.58, aligning with Fioruci, Ehlers, and Andrade Filho (2014). We obtained a Bayes estimate of the conditional precision matrix of $\hat{\mathbf{P}}_t = \mathbb{E}[\mathbf{P}_t|\mathbf{Z}]$ and a conditional inverse correlation matrix of $\hat{\mathbf{S}}_t = \mathbb{E}[\mathbf{S}_t|\mathbf{Z}]$ as posterior means.

In each of the Monte Carlo designs, we evaluated the accuracy of the estimated conditional precision matrices and conditional inverse correlation matrices by computing their spectral and Frobenius norms of deviation from the true matrices, $\mathbf{P}^0_t$ and $\mathbf{S}^0_t$, respectively. We measured the performance using the ratio of norm loss averages (RNLA) for the conditional precision matrix, defined as,

$$\text{RNLA}_{\mathbf{P}}(J) \equiv \left\{ \frac{\sum_{r=1}^{R} \sum_{t=1}^{T} ||\tilde{\mathbf{P}}^{(r)}_{t,j} - \mathbf{P}^0_t||}{\sum_{r=1}^{R} \sum_{t=1}^{T} ||\hat{\mathbf{P}}_t^{\,(r)} - \mathbf{P}^0_t||} \right\} \tag{4.2}$$

for each spectral and Frobenius norm, and similarly, as

$$\text{RNLA}_{\mathbf{S}}(J) \equiv \left\{ \frac{\sum_{r=1}^{R} \sum_{t=1}^{T} \left\|\tilde{\mathbf{S}}^{(r)}_{t,j} - \mathbf{S}^0_t\right\|}{\sum_{r=1}^{R} \sum_{t=1}^{T} \left\|\hat{\mathbf{S}}_t^{\,(r)} - \mathbf{S}^0_t\right\|} \right\}, \tag{4.3}$$

for the conditional inverse correlation matrix, where $J = (j)$ includes DCC-NL (Engle, Ledoit, and Wolf, 2019), DCC-L (Ledoit and Wolf, 2004b), Gaussian Copula, and t-Copula (Patton, 2009) estimators. $\tilde{\mathbf{P}}^{(r)}_{t,j} \equiv \hat{\mathbf{\Sigma}}^{-1,(r)}_{t,j}$ and $\tilde{\mathbf{S}}_{t,j} = \hat{\mathbf{R}}^{-1,(r)}_{t,j}$ are estimators of $\mathbf{P}^0_t$ and $\mathbf{S}^0_t$ obtained by inverting the estimated conditional covariance and correlation matrices using the estimation methods in J. An RNLA(J) above 1 indicates that, on average, the proposed method outperforms the J method, whereas an RNLA below 1 suggests the inferior performance of our proposed method compared to method in J.

4.1.1 Monte Carlo design A

Table 1 summarizes the results for Monte Carlo design A, and provide both spectral and Frobenius norm comparisons for the Bayesian nonparanormal conditional estimators and the DCC-NL

Table 1: Spectral and Frobenius norm losses for the different conditional precision and inverse correlation matrices estimators – Monte Carlo design A

	Bayesian nonparanormal conditional estimator								DCC-NL							
Norms	**Spectral**				**Frobenius**				**Spectral**				**Frobenius**			
T\N	25	50	100	125	25	50	100	125	25	50	100	125	25	50	100	125
	Error distribution: ε_{it} ∼Gaussian															
	Conditional precision matrix															
50	1.276	1.320	1.982	2.332	2.829	3.864	5.970	7.062	2.529	2.780	3.178	3.188	4.949	6.931	9.716	10.375
100	1.180	1.142	1.549	1.862	2.667	3.695	5.769	6.904	1.972	2.268	2.541	2.499	4.273	6.158	8.763	9.189
150	1.156	1.099	1.551	1.692	2.613	3.604	5.706	6.625	1.848	2.138	2.379	2.265	4.044	5.956	8.274	8.791
200	1.140	1.055	1.425	1.638	2.580	3.496	5.411	6.386	1.803	2.048	2.282	2.227	4.031	5.830	8.245	8.785
250	1.137	1.043	1.332	1.541	2.549	3.434	5.235	6.187	1.768	1.975	2.160	2.296	3.965	5.705	7.991	9.168
	Conditional inverse correlation matrix															
50	1.938	2.054	2.126	2.159	4.059	5.711	7.913	8.883	2.025	2.199	2.344	2.380	4.242	6.071	8.650	9.670
100	1.941	2.038	2.098	2.117	4.062	5.649	7.770	8.628	2.023	2.197	2.343	2.381	4.231	6.059	8.630	9.676
150	1.940	2.040	2.100	2.116	4.054	5.622	7.772	8.626	2.022	2.198	2.347	2.382	4.229	6.061	8.648	9.687
200	1.936	2.037	2.095	2.113	4.048	5.620	7.779	8.618	2.022	2.198	2.341	2.383	4.229	6.062	8.624	9.696
250	1.934	2.038	2.099	2.116	4.039	5.616	7.758	8.602	2.021	2.198	2.346	2.380	4.225	6.059	8.645	9.662
	Error distribution: $\varepsilon_{it} \sim t$-distributed with 3 degrees of freedom															
	Conditional precision matrix															
50	1.521	2.476	4.119	4.601	3.210	5.198	8.939	10.659	4.465	4.657	5.853	5.716	8.704	11.070	17.515	18.194
100	1.337	1.872	2.971	3.480	2.966	4.630	7.917	9.509	3.701	3.462	4.650	4.696	7.435	9.012	14.825	16.026
150	1.254	1.761	2.719	2.934	2.862	4.453	7.548	8.970	3.250	3.122	4.244	3.957	6.595	8.338	13.554	14.192
200	1.200	1.490	2.333	2.878	2.742	4.133	7.086	8.446	2.893	2.886	3.939	3.895	6.275	7.930	13.050	13.699
250	1.176	1.433	2.298	2.489	2.688	4.022	6.912	7.934	2.908	2.823	3.677	3.740	6.168	7.699	12.283	13.781
	Conditional inverse correlation matrix															
50	1.970	2.097	2.148	2.162	4.191	6.008	8.145	8.963	2.034	2.205	2.349	2.385	4.263	6.090	8.674	9.722
100	1.947	2.064	2.119	2.123	4.094	5.807	7.889	8.693	2.031	2.203	2.347	2.397	4.254	6.076	8.648	9.800
150	1.946	2.073	2.112	2.140	4.078	5.827	7.915	8.904	2.028	2.204	2.351	2.389	4.246	6.080	8.699	9.740
200	1.940	2.054	2.115	2.128	4.062	5.721	7.970	8.791	2.029	2.202	2.346	2.392	4.248	6.071	8.662	9.745
250	1.938	2.056	2.124	2.134	4.049	5.720	8.015	8.779	2.028	2.201	2.349	2.384	4.244	6.073	8.670	9.675

Notes: The average norm losses, computed over 100 replicates ($R = 100$), are given for both spectral and Frobenius norms. For the conditional precision matrix ($\mathbf{P}_t^0$) and the conditional inverse correlation matrix ($\mathbf{S}_t^0$), they are $\frac{1}{R}\frac{1}{T}\sum_{r=1}^{R}\sum_{t=1}^{T}||\mathring{\mathbf{P}}_t^{(r)} - \mathbf{P}_t^0||$ and $\frac{1}{R}\frac{1}{T}\sum_{r=1}^{R}\sum_{t=1}^{T}||\mathring{\mathbf{S}}_t^{(r)} - \mathbf{S}_t^0||$, where $\mathring{\mathbf{P}}_t^{(r)} = \{\hat{\mathbf{P}}_t^{(r)}, \hat{\mathbf{\Sigma}}_t^{-1,(r)}\}$ and $\mathring{\mathbf{S}}_t^{(r)} = \{\hat{\mathbf{S}}_t^{(r)}, \hat{\mathbf{R}}_t^{-1}\}$. $\hat{\mathbf{P}}_t^{(r)}$ and $\hat{\mathbf{S}}_t^{(r)}$ are the Bayesian nonparanormal conditional estimators. $\hat{\mathbf{\Sigma}}_t^{(r)}$ and $\hat{\mathbf{R}}_t^{(r)}$ are DCC-NL estimators of the conditional precision and inverse correlation matrices of Engle, Ledoit, and Wolf (2019).

estimator. First, we note that the Bayesian method dominates the DCC-NL estimators in both conditional precision and inverse correlation matrices. Both methods reveal that the loss of norms decreases with increased sample size. This observation holds even when the error term is non-Gaussian. Based on the values of the losses of the norms, Tables 2 and 3 will show RNLAs for the different conditional precision and inverse correlation matrix estimators.

Table 2 provides an evaluation of the Bayesian nonparanormal conditional precision and inverse correlation matrix estimator's performance through the RNLAs defined in Equations (4.2) and (4.3). If the value of the RNLA is greater than 1, it implies the outperformance of our proposed estimator. For both the spectral and Frobenius norms, our proposed estimator outperform over both the DCC–L and DCC–NL methods irrespective of the distribution of the error terms or sample size combinations. First, it can be observed that the RNLA value decreases as the number of samples, T, increases in the spectral and Frobenius norms of the conditional precision matrices, which is more pronounced in RNLA with DCC-NL estimators.

Table 2: Ratio of spectral and Frobenius norm loss averages for the different conditional precision matrix estimators and inverse correlation matrices estimators (DCC–NL and DCC–L models) – Monte Carlo design A

J	DCC-NL								DCC-L							
Norms	**Spectral**				**Frobenius**				**Spectral**				**Frobenius**			
T\N	25	50	100	125	25	50	100	125	25	50	100	125	25	50	100	125
	Error distribution: $\varepsilon_{it} \sim$Gaussian															
	Relative norms of conditional precision matrix															
50	1.983	2.106	1.603	1.367	1.750	1.794	1.627	1.469	1.946	2.165	1.632	1.373	1.738	1.860	1.671	1.483
100	1.670	1.986	1.640	1.343	1.602	1.666	1.519	1.331	1.678	2.080	1.830	1.340	1.601	1.739	1.705	1.330
150	1.598	1.945	1.535	1.338	1.547	1.653	1.450	1.327	1.608	2.058	1.570	1.333	1.550	1.738	1.492	1.322
200	1.581	1.942	1.602	1.360	1.563	1.667	1.524	1.376	1.605	2.079	1.882	1.350	1.574	1.760	1.785	1.370
250	1.555	1.894	1.622	1.489	1.555	1.661	1.527	1.482	1.580	2.049	1.695	1.842	1.567	1.764	1.596	1.820
	Relative norms of conditional inverse correlation matrix															
50	1.045	1.070	1.103	1.102	1.045	1.063	1.093	1.089	1.047	1.082	1.111	1.105	1.053	1.093	1.115	1.094
100	1.042	1.078	1.117	1.125	1.041	1.073	1.111	1.121	1.045	1.090	1.140	1.125	1.052	1.105	1.171	1.124
150	1.042	1.078	1.117	1.126	1.043	1.078	1.113	1.123	1.046	1.091	1.126	1.126	1.054	1.112	1.140	1.127
200	1.044	1.079	1.117	1.128	1.045	1.079	1.109	1.125	1.048	1.093	1.146	1.129	1.057	1.114	1.186	1.130
250	1.045	1.078	1.118	1.125	1.046	1.079	1.114	1.123	1.049	1.093	1.129	1.159	1.058	1.116	1.147	1.219
	Error distribution: $\varepsilon_{it} \sim t$-distributed with 3 degrees of freedom															
	Relative norms of conditional precision matrix															
50	2.936	1.881	1.421	1.242	2.712	2.130	1.959	1.707	3.514	4.435	3.138	2.422	3.087	3.575	3.099	2.588
100	2.769	1.849	1.565	1.349	2.506	1.946	1.872	1.685	3.104	3.830	3.567	2.300	2.766	2.982	3.116	2.151
150	2.591	1.773	1.561	1.349	2.304	1.872	1.796	1.582	2.761	3.527	2.683	2.195	2.486	2.800	2.408	2.071
200	2.412	1.936	1.688	1.353	2.288	1.919	1.842	1.622	2.534	3.418	3.216	2.197	2.414	2.730	2.805	2.060
250	2.473	1.969	1.600	1.503	2.295	1.914	1.777	1.737	2.525	3.375	2.833	3.064	2.390	2.677	2.417	2.810
	Relative norms of conditional inverse correlation matrix															
50	1.032	1.052	1.094	1.103	1.017	1.014	1.065	1.085	1.039	1.073	1.121	1.108	1.039	1.065	1.137	1.103
100	1.043	1.068	1.107	1.129	1.039	1.046	1.096	1.127	1.048	1.087	1.158	1.128	1.055	1.096	1.214	1.130
150	1.043	1.063	1.113	1.117	1.041	1.043	1.099	1.094	1.045	1.080	1.131	1.128	1.053	1.087	1.154	1.131
200	1.046	1.072	1.109	1.124	1.046	1.061	1.087	1.109	1.050	1.088	1.150	1.131	1.058	1.103	1.199	1.134
250	1.047	1.070	1.106	1.117	1.048	1.062	1.082	1.102	1.049	1.084	1.130	1.166	1.059	1.099	1.153	1.239

Notes: The Ratio of Spectral and Frobenius Norm Loss Averages (RNLA) for both Spectral and Frobenius norms are computed from 100 replications ($R = 100$): $\text{RNLA}_{\mathbf{P}}(J) = \{\sum_{r=1}^{R}\sum_{t=1}^{T}||\tilde{\mathbf{P}}_{t,j}^{(r)} - \mathbf{P}_t^0||/\sum_{r=1}^{R}\sum_{t=1}^{T}||\hat{\mathbf{P}}_t^{(r)} - \mathbf{P}_t^0||\}$ and $\text{RNLA}_{\mathbf{S}}(J) = \{\sum_{r=1}^{R}\sum_{t=1}^{T}||\tilde{\mathbf{S}}_{t,j}^{(r)} - \mathbf{S}_t^0||/\sum_{r=1}^{R}\sum_{t=1}^{T}||\hat{\mathbf{S}}_t^{(r)} - \mathbf{S}_t^0||\}$, and $J =$ DCC–L and DCC–NL of Ledoit and Wolf (2004b) and Engle, Ledoit, and Wolf (2019), where $\hat{\mathbf{P}}_t$ and $\hat{\mathbf{S}}_t$ denote the posterior mean of the conditional precision and inverse correlation matrices derived from the Bayesian approach we suggest, while $\mathbf{P}_t^0$ and $\mathbf{S}_t^0$refers to the known true conditional precision and inverse correlation matrices.

The DCC-L estimator shows similar results to the DCC-NL estimator when $N = 25$, but if T is not large enough for the number of variables, N, DCC-L shows an increased RNLA. As N increases, there is a decrease in most of the RNLA values, though this decrease is not the same for all Ts. This implies that with an increase in N, the results from both DCC-L and DCC-NL are likely to align more closely with those obtained from our proposed estimation method. When estimating conditional inverse correlation matrices, an increase in both N and T leads to an increase in RNLA. It is even more pronounced in non-Gaussian distribution. When DCC-NL and DCC-L are compared, DCC-NL shows better results than DCC-L regardless of the number of variables and sample size. This difference can be seen better in the case of non-Gaussian distribution.

Table 3 presents the RNLA values for both the conditional precision and inverse correlation

Table 3: Ratio of spectral and Frobenius norm loss averages for the different conditional precision matrix estimators, $\mathbf{P}_t$, and inverse correlation matrix estimators, $\mathbf{S}_t$ (Gaussian and t-Copula models) – Monte Carlo design A

J	Gaussian Copula								t-Copula							
Norms	**Spectral**				**Frobenius**				**Spectral**				**Frobenius**			
T\N	25	50	100	125	25	50	100	125	25	50	100	125	25	50	100	125
	Error distribution: $\varepsilon_{it} \sim$Gaussian															
	Relative norms of conditional precision matrix															
50	9.040	n/a	n/a	n/a	5.956	n/a	n/a	n/a	15.769	n/a	n/a	n/a	10.205	n/a	n/a	n/a
100	3.536	9.790	n/a	n/a	2.818	5.648	n/a	n/a	6.362	9.833	n/a	n/a	4.831	5.660	n/a	n/a
150	2.732	5.310	18.296	70.618	2.305	3.542	9.721	28.530	4.530	5.302	18.129	69.953	3.723	3.548	9.629	28.250
200	2.461	4.129	7.927	13.163	2.149	2.930	5.208	7.832	3.860	4.163	7.850	13.020	3.385	2.969	5.153	7.741
250	2.232	3.497	5.668	7.531	2.029	2.621	3.972	5.070	3.739	3.542	5.617	7.449	3.269	2.668	3.927	5.008
	Relative norms of conditional inverse correlation matrix															
50	1.657	n/a	n/a	n/a	1.567	n/a	n/a	n/a	1.700	n/a	n/a	n/a	1.572	n/a	n/a	n/a
100	1.124	1.847	n/a	n/a	1.239	1.616	n/a	n/a	1.122	1.853	n/a	n/a	1.240	1.618	n/a	n/a
150	1.091	1.245	3.396	6.959	1.162	1.383	2.111	3.061	1.089	1.241	3.393	6.959	1.159	1.382	2.110	3.061
200	1.080	1.151	2.006	2.953	1.130	1.289	1.682	1.990	1.081	1.152	2.002	2.950	1.133	1.292	1.680	1.988
250	1.071	1.134	1.514	2.020	1.110	1.238	1.522	1.704	1.073	1.136	1.511	2.016	1.113	1.241	1.520	1.701
	Error distribution: $\varepsilon_{it} \sim t$-distributed with 3 degrees of freedom															
	Relative norms of conditional precision matrix															
50	7.471	n/a	n/a	n/a	5.166	n/a	n/a	n/a	12.095	n/a	n/a	n/a	8.174	n/a	n/a	n/a
100	3.128	8.732	n/a	n/a	2.538	6.210	n/a	n/a	6.177	9.573	n/a	n/a	4.609	6.932	n/a	n/a
150	2.542	4.794	15.852	51.00	2.133	3.887	11.195	27.652	4.871	5.763	13.775	46.750	3.717	4.688	9.710	25.294
200	2.387	4.079	8.375	12.27	2.071	3.351	6.622	9.498	4.355	5.252	7.411	10.444	3.518	4.115	5.865	8.062
250	2.213	3.523	6.105	7.96	1.988	2.906	5.329	6.637	4.117	4.633	5.138	6.610	3.358	3.735	4.479	5.485
	Relative norms of conditional inverse correlation matrix															
50	1.632	n/a	n/a	n/a	1.519	n/a	n/a	n/a	1.647	n/a	n/a	n/a	1.521	n/a	n/a	n/a
100	1.122	1.832	n/a	n/a	1.233	1.572	n/a	n/a	1.130	1.825	n/a	n/a	1.246	1.580	n/a	n/a
150	1.091	1.237	3.312	6.449	1.161	1.338	2.078	2.905	1.103	1.221	9.710	6.456	1.176	1.339	2.071	2.904
200	1.083	1.141	1.994	2.977	1.134	1.270	1.655	1.965	1.095	1.148	5.865	2.963	1.149	1.276	1.648	1.957
250	1.076	1.118	1.505	2.035	1.117	1.210	1.486	1.685	1.089	1.132	4.479	2.017	1.131	1.226	1.474	1.673

Notes: The Ratio of Spectral and Frobenius Norm Loss Averages (RNLA) for both Spectral and Frobenius norms are computed from 100 replications ($R = 100$): $\text{RNLA}_{\mathbf{P}}(J) = \{\sum_{r=1}^{R}\sum_{t=1}^{T}||\tilde{\mathbf{P}}_{t,j}^{(r)} - \mathbf{P}_t^0||/\sum_{r=1}^{R}\sum_{t=1}^{T}||\hat{\mathbf{P}}_t^{(r)} - \mathbf{P}_t^0||\}$ and $\text{RNLA}_{\mathbf{S}}(J) = \{\sum_{r=1}^{R}\sum_{t=1}^{T}||\tilde{\mathbf{S}}_{t,j}^{(r)} - \mathbf{S}_t^0||/\sum_{r=1}^{R}\sum_{t=1}^{T}||\hat{\mathbf{S}}_t^{(r)} - \mathbf{S}_t^0||\}$, and J = Gaussian Copula and t-Copula of Patton (2009), where $\hat{\mathbf{P}}_t$ and $\hat{\mathbf{S}}_t$ denote the posterior mean of the conditional precision and inverse correlation matrices derived from the Bayesian approach we suggest, while $\mathbf{P}_t^0$ and $\mathbf{S}_t^0$refers to the known true conditional precision and inverse correlation matrices. Gaussian and t-Copula models lack regularization or shrinkage methods within their estimation procedures. These models fail to yield estimates in the singular case ($T < N$). Such instances are denoted as 'not applicable' (n/a).

matrix estimators for Gaussian Copula and t-Copula. Our proposed estimator produces better estimation results than Gaussian Copula and t-Copula as the number of variables increases. However, if T is significantly large relative to N, it can be seen that RNLA decreases regardless of the error distribution. Neither Gaussian Copula nor t-Copula assume a situation where the size of the sample is larger than the number of variables, so they do not use shrinkage or regularization methodologies in estimating the unconditional correlation matrix. Therefore, when $N > T$, it is denoted as n/a. When compared with DCC-L and DCC-NL based on the relative size of RNLA, for example, with the exception of Gaussian Copula in the non-Gaussian distribution, DCC-L and DCC-NL provide better estimates in most cases. When comparing Gaussian Copula and t-Coupla, it can be seen that Gaussian Copula shows better performance regardless of the distribution of error terms, or N and T combinations in estimating the con-

ditional precision matrix. On the other hand, in the case of conditional inverse correlation, a slight difference in performance can be observed, but the difference disappears as T increases.

Results based on the Monte Carlo design A illustrate the effectiveness of estimating the conditional precision and inverse correlation matrices under relatively stable eigenvalue distributions instead of inverting the estimated conditional covariance and conditional correlation matrices.

4.1.2 Monte Carlo design B

Table 4: Spectral and Frobenius norm losses for the different conditional precision and inverse correlation matrices estimators – Monte Carlo design B

	Bayesian nonparanormal conditional estimator								**DCC-NL**							
Norms	**Spectral**				**Frobenius**				**Spectral**				**Frobenius**			
T\N	25	50	100	125	25	50	100	125	25	50	100	125	25	50	100	125
	Error distribution: $\varepsilon_{it} \sim$Gaussian															
	Conditional precision matrix															
50	23.74	39.55	68.31	81.99	50.81	102.41	228.00	299.43	22.99	38.92	67.88	81.58	47.68	98.96	224.63	296.08
100	29.78	45.64	74.87	89.31	73.80	134.41	273.08	352.90	29.27	45.17	74.49	89.05	71.45	131.52	269.95	350.22
150	35.99	52.00	81.83	95.71	97.84	167.68	320.91	403.65	35.59	51.61	81.50	95.43	95.96	165.23	318.17	401.05
200	42.04	58.11	88.21	102.17	122.10	201.39	367.76	456.01	41.71	57.78	87.90	101.90	120.51	199.22	365.11	453.60
250	48.06	64.57	94.79	109.30	146.56	235.98	415.60	510.59	47.78	64.28	94.53	109.04	145.17	234.04	413.33	508.05
	Conditional inverse correlation matrix															
50	1.30	1.91	2.64	2.89	2.93	5.32	9.05	10.67	1.31	1.91	2.64	2.89	2.93	5.26	9.06	10.66
100	1.05	1.46	2.08	2.31	2.34	4.24	7.59	9.08	1.03	1.48	2.09	2.32	2.32	4.27	7.63	9.13
150	0.94	1.24	1.76	1.97	2.02	3.69	6.69	8.07	0.91	1.27	1.79	1.98	2.00	3.70	6.77	8.15
200	0.85	1.10	1.55	1.74	1.80	3.31	6.06	7.35	0.85	1.15	1.58	1.76	1.80	3.32	6.11	7.45
250	0.79	1.02	1.40	1.58	1.65	3.03	5.58	6.82	0.81	1.07	1.44	1.60	1.65	3.04	5.67	6.85
	Error distribution: $\varepsilon_{it} \sim t$-distributed with 3 degrees of freedom															
	Conditional precision matrix															
50	23.68	39.34	68.00	82.43	50.58	101.85	227.03	300.92	22.40	38.44	67.18	81.84	45.38	96.84	221.06	295.76
100	29.83	45.58	74.78	89.53	73.72	134.25	272.90	353.38	28.80	44.79	73.99	88.87	68.99	129.53	266.60	347.48
150	35.86	51.99	81.64	95.23	97.48	167.51	320.24	401.70	35.045	51.35	80.94	94.72	93.62	163.55	314.42	396.48
200	41.99	58.14	88.27	102.57	121.69	201.01	367.50	456.61	41.29	57.60	87.67	101.95	118.27	197.64	362.10	451.29
250	47.96	64.47	94.72	109.29	146.01	235.19	415.00	510.16	47.35	64.09	94.19	108.77	143.00	232.47	410.34	505.06
	Conditional inverse correlation matrix															
50	1.36	1.95	2.63	2.90	3.14	5.61	9.08	10.74	1.33	1.91	2.64	2.90	2.95	5.30	9.08	10.70
100	1.05	1.49	2.09	2.32	2.37	4.47	7.73	9.19	1.06	1.49	2.09	2.33	2.36	4.30	7.65	9.24
150	0.93	1.29	1.79	1.99	2.05	4.01	6.98	8.31	0.95	1.28	1.79	1.99	2.04	3.73	6.83	8.21
200	0.87	1.15	1.61	1.77	1.83	3.60	6.57	7.70	0.90	1.16	1.59	1.77	1.85	3.34	6.17	7.52
250	0.83	1.08	1.46	1.60	1.68	3.28	6.10	7.07	0.85	1.09	1.45	1.60	1.70	3.07	5.71	6.86

Notes: The average norm losses, computed over 100 replicates ($R = 100$), are given for both spectral and Frobenius norms. For the conditional precision matrix ($\mathbf{P}_t^0$) and the conditional inverse correlation matrix ($\mathbf{S}_t^0$), they are $\frac{1}{R}\frac{1}{T}\sum_{r=1}^{R}\sum_{t=1}^{T}||\mathring{\mathbf{P}}_t^{(r)} - \mathbf{P}_t^0||$ and $\frac{1}{R}\frac{1}{T}\sum_{r=1}^{R}\sum_{t=1}^{T}||\mathring{\mathbf{S}}_t^{(r)} - \mathbf{S}_t^0||$, where $\mathring{\mathbf{P}}_t^{(r)} = \{\hat{\mathbf{P}}_t^{(r)}, \hat{\mathbf{\Sigma}}_t^{-1,(r)}\}$ and $\mathring{\mathbf{S}}_t^{(r)} = \{\hat{\mathbf{S}}_t^{(r)}, \hat{\mathbf{R}}_t^{-1}\}$. $\hat{\mathbf{P}}_t^{(r)}$ and $\hat{\mathbf{S}}_t^{(r)}$ are the Bayesian nonparanormal conditional estimators. $\hat{\mathbf{\Sigma}}_t^{(r)}$ and $\hat{\mathbf{R}}_t^{(r)}$ are DCC-NL estimators of the conditional precision and inverse correlation matrices of Engle, Ledoit, and Wolf (2019).

Table 4 presents the norm losses for Bayesian nonparanormal conditional estimators of the conditional inverse correlation matrix for Monte Carlo design B. Our findings show that both the Bayesian nonparanormal conditional estimator and the DCC-NL estimator fail to accurately estimate the conditional precision matrix due to their unstable eigenvalue distribution in Monte Carlo design B. Conversely, we can still estimate the conditional inverse correlation with

widely distributed eigenvalues by stabilizing the distribution through rescailng in the estimated precision matrix. Thus, our proposed estimator yields norms comparable to the DCC-NL and outperforms scaled estimates like conditional partial correlation, even under these conditions. Based on the values of the losses of the norms, Tables 5 and 6 will show RNLAs for the different conditional precision and inverse correlation matrix estimators.

Table 5: Ratio of spectral and Frobenius norm loss averages for the different conditional precision matrix estimators and inverse correlation matrices estimators (DCC–NL and DCC–L models) – Monte Carlo design B

J	DCC-NL								DCC-L							
Norms	**Spectral**				**Frobenius**				**Spectral**				**Frobenius**			
T\N	25	50	100	125	25	50	100	125	25	50	100	125	25	50	100	125
	Error distribution: ε_{it} ∼Gaussian															
	Relative norms of conditional precision matrix															
50	0.969	0.984	0.994	0.995	0.938	0.966	0.985	0.989	0.969	0.984	0.993	0.996	0.939	0.965	0.985	0.989
100	0.983	0.990	0.995	0.997	0.968	0.979	0.989	0.992	0.983	0.989	0.995	0.996	0.968	0.977	0.987	0.992
150	0.989	0.993	0.996	0.997	0.981	0.985	0.991	0.994	0.989	0.992	0.996	0.997	0.981	0.984	0.991	0.994
200	0.992	0.994	0.997	0.997	0.987	0.989	0.993	0.995	0.992	0.993	0.995	0.998	0.986	0.987	0.990	0.995
250	0.994	0.995	0.997	0.998	0.991	0.992	0.995	0.995	0.994	0.995	0.997	0.996	0.990	0.990	0.994	0.992
	Relative norms of conditional inverse correlation matrix															
50	1.006	1.001	1.002	1.000	1.000	0.990	1.002	1.000	1.006	1.015	1.006	1.001	1.023	1.027	1.015	1.002
100	0.982	1.015	1.006	1.003	0.993	1.007	1.006	1.005	0.973	1.041	1.031	1.003	1.047	1.084	1.073	1.008
150	0.967	1.024	1.012	1.006	0.992	1.001	1.011	1.010	0.952	1.061	1.027	1.007	1.075	1.127	1.059	1.016
200	0.995	1.039	1.018	1.011	0.998	1.005	1.008	1.014	0.968	1.073	1.079	1.012	1.109	1.163	1.172	1.025
250	1.022	1.055	1.033	1.014	1.002	1.005	1.016	1.003	0.982	1.080	1.060	1.086	1.122	1.187	1.112	1.200
	Error distribution: $\varepsilon_{it} \sim t$-distributed with 3 degrees of freedom															
	Relative norms of conditional precision matrix															
50	0.946	0.977	0.988	0.993	0.897	0.951	0.974	0.983	0.943	0.966	0.982	0.997	0.893	0.934	0.968	0.987
100	0.966	0.983	0.989	0.993	0.936	0.965	0.977	0.983	0.967	0.976	0.985	0.995	0.935	0.952	0.971	0.986
150	0.977	0.988	0.992	0.995	0.960	0.976	0.982	0.987	0.974	0.983	0.988	0.990	0.957	0.966	0.979	0.983
200	0.983	0.991	0.993	0.994	0.972	0.983	0.985	0.988	0.982	0.987	0.991	0.998	0.968	0.974	0.980	0.990
250	0.987	0.994	0.994	0.995	0.979	0.988	0.989	0.990	0.985	0.989	0.993	0.993	0.976	0.979	0.986	0.985
	Relative norms of conditional inverse correlation matrix															
50	0.976	0.984	1.002	1.000	0.940	0.945	0.999	0.997	1.034	1.029	1.009	1.004	1.068	1.064	1.029	1.008
100	1.016	0.998	1.001	1.004	0.997	0.960	0.990	1.005	1.009	1.066	1.048	1.003	1.091	1.137	1.125	1.013
150	1.012	0.993	1.002	1.001	0.996	0.930	0.978	0.987	0.984	1.079	1.035	1.008	1.101	1.159	1.079	1.021
200	1.037	1.008	0.989	1.000	1.013	0.927	0.938	0.976	1.010	1.089	1.087	1.017	1.138	1.184	1.195	1.032
250	1.028	1.009	0.997	1.003	1.009	0.936	0.937	0.971	1.022	1.089	1.067	1.096	1.143	1.191	1.123	1.233

Notes: The Ratio of Spectral and Frobenius Norm Loss Averages (RNLA) for both Spectral and Frobenius norms are computed from 100 replications ($R = 100$): $\text{RNLA}_{\mathbf{P}}(J) = \{\sum_{r=1}^{R}\sum_{t=1}^{T}||\tilde{\mathbf{P}}_{t,j}^{(r)} - \mathbf{P}_t^0||/\sum_{r=1}^{R}\sum_{t=1}^{T}||\hat{\mathbf{P}}_t^{(r)} - \mathbf{P}_t^0||\}$ and $\text{RNLA}_{\mathbf{S}}(J) = \{\sum_{r=1}^{R}\sum_{t=1}^{T}||\tilde{\mathbf{S}}_{t,j}^{(r)} - \mathbf{S}_t^0||/\sum_{r=1}^{R}\sum_{t=1}^{T}||\hat{\mathbf{S}}_t^{(r)} - \mathbf{S}_t^0||\}$, and J = DCC–L and DCC–NL of Ledoit and Wolf (2004b) and Engle, Ledoit, and Wolf (2019), where $\hat{\mathbf{P}}_t$ and $\hat{\mathbf{S}}_t$ denote the posterior mean of the conditional precision and inverse correlation matrices derived from the Bayesian approach we suggest, while $\mathbf{P}_t^0$ and $\mathbf{S}_t^0$refers to the known true conditional precision and inverse correlation matrices.

Tables 5 and 6 show the RNLA values for each estimator. First, as Table 4 shows, Monte Carlo design B shows that no estimator we consider gives a sufficient estimation of the conditional precision matrix. Therefore, in Tables 5 and 6, we will focus more on the result of the conditional inverse correlation. As shown in Table 5, irrespective of the error term distribution, in most cases, our proposed estimation method gives comparable results with DCC–NL and slightly better performance than DCC–L in estimating the conditional inverse correlation

matrix. However, no clear ordering emerges when we compare DCC–NL and DCC–L.

Table 6: Ratio of spectral and Frobenius norm loss averages for the different conditional precision matrix estimators and inverse correlation matrices estimators (Gaussian and t-Copula models) – Monte Carlo design B

J	**Gaussian Copula estimator**								**t-Copula estimator**							
Norms	**Spectral**				**Frobenius**				**Spectral**				**Frobenius**			
T\N	25	50	100	125	25	50	100	125	25	50	100	125	25	50	100	125
	Error distribution: ε_{it} ∼Gaussian															
	Relative norms of conditional precision matrix															
50	0.936	n/a	n/a	n/a	0.897	n/a	n/a	n/a	0.969	n/a	n/a	n/a	0.920	n/a	n/a	n/a
100	0.971	0.970	n/a	n/a	0.944	0.939	n/a	n/a	0.951	0.970	n/a	n/a	0.901	0.939	n/a	n/a
150	0.981	0.982	0.975	1.141	0.967	0.964	0.951	0.995	0.961	0.982	0.976	1.135	0.934	0.964	0.952	0.994
200	0.987	0.987	0.985	0.983	0.977	0.976	0.969	0.964	0.976	0.988	0.986	0.983	0.954	0.976	0.970	0.964
250	0.990	0.990	0.990	0.988	0.984	0.982	0.979	0.976	0.976	0.991	0.990	0.989	0.961	0.982	0.979	0.976
	Relative norms of conditional inverse correlation matrix															
50	2.426	n/a	n/a	n/a	1.908	n/a	n/a	n/a	2.465	n/a	n/a	n/a	1.910	n/a	n/a	n/a
100	1.540	2.552	n/a	n/a	1.527	1.903	n/a	n/a	1.545	2.550	n/a	n/a	1.526	1.902	n/a	n/a
150	1.296	1.913	4.030	7.406	1.424	1.652	2.316	3.195	1.289	1.912	4.027	7.404	1.412	1.651	2.314	3.195
200	1.197	1.656	2.669	3.550	1.381	1.565	1.909	2.175	1.224	1.654	2.663	3.546	1.387	1.563	1.906	2.173
250	1.118	1.496	2.218	2.679	1.343	1.505	1.765	1.900	1.133	1.493	2.213	2.674	1.366	1.501	1.760	1.896
	Error distribution: $\varepsilon_{it} \sim t$-distributed with 3 degrees of freedom															
	Relative norms of conditional precision matrix															
50	0.939	n/a	n/a	n/a	0.902	n/a	n/a	n/a	0.968	n/a	n/a	n/a	0.930	n/a	n/a	n/a
100	0.969	0.954	n/a	n/a	0.945	0.915	n/a	n/a	0.950	0.958	n/a	n/a	0.905	0.920	n/a	n/a
150	0.985	0.968	0.966	1.407	0.970	0.936	0.939	1.038	0.967	0.970	0.970	1.296	0.939	0.940	0.944	1.021
200	0.987	0.975	0.976	0.973	0.980	0.951	0.949	0.946	0.974	0.977	0.979	0.978	0.954	0.956	0.956	0.954
250	0.991	0.980	0.980	0.980	0.986	0.962	0.960	0.958	0.980	0.982	0.984	0.984	0.966	0.967	0.968	0.967
	Relative norms of conditional inverse correlation matrix															
50	2.311	n/a	n/a	n/a	1.777	n/a	n/a	n/a	2.329	n/a	n/a	n/a	1.780	n/a	n/a	n/a
100	1.562	2.531	n/a	n/a	1.513	1.829	n/a	n/a	1.578	2.526	n/a	n/a	1.544	1.825	n/a	n/a
150	1.315	1.811	3.898	7.031	1.423	1.538	2.228	3.055	1.357	1.805	3.886	7.040	1.472	1.532	2.220	3.054
200	1.202	1.606	2.582	3.543	1.394	1.475	1.779	2.093	1.277	1.588	2.568	3.526	1.453	1.458	1.769	2.083
250	1.105	1.458	2.126	2.679	1.362	1.446	1.633	1.857	1.234	1.431	2.102	2.655	1.430	1.416	1.614	1.841

Notes: The Ratio of Spectral and Frobenius Norm Loss Averages (RNLA) for both Spectral and Frobenius norms are computed from 100 replications ($R = 100$): $\text{RNLA}_{\mathbf{P}}(J) = (\sum_{r=1}^{R}\sum_{t=1}^{T}||\tilde{\mathbf{P}}_{t,j}^{(r)} - \mathbf{P}_t^0||/\sum_{r=1}^{R}\sum_{t=1}^{T}||\hat{\mathbf{P}}_t{}^{(r)} - \mathbf{P}_t^0||\}$ and $\text{RNLA}_{\mathbf{S}}(J) = \{\sum_{r=1}^{R}\sum_{t=1}^{T}||\tilde{\mathbf{S}}_{t,j}^{(r)} - \mathbf{S}_t^0||/\sum_{r=1}^{R}\sum_{t=1}^{T}||\hat{\mathbf{S}}_t{}^{(r)} - \mathbf{S}_t^0||\}$, and J = Gaussian Copula and t-Copula of Patton (2009), where $\hat{\mathbf{P}}_t$ and $\hat{\mathbf{S}}_t$ denote the posterior mean of the conditional precision and inverse correlation matrices derived from the Bayesian approach we suggest, while $\mathbf{P}_t^0$ and $\mathbf{S}_t^0$refers to the known true conditional precision and inverse correlation matrices. Gaussian and t-Copula models lack regularization or shrinkage methods within their estimation procedures. These models fail to yield estimates in the singular case ($T < N$). Such instances are denoted as 'not applicable' (n/a).

Similarly, in Table 6, our proposed estimator shows better performance than Gaussian Copula and t-Copula in estimating conditional inverse correlation. When compared with other variables, both Gaussian Copula and t-Copula gave higher RNLA values for all norm values compared to DCC-L and DCC-NL when the sample size was insufficient for the number of variables.

In the context of Monte Carlo design B, the simulation results demonstrate that estimating the conditional inverse correlation matrix is not only feasible but also yields competitive performance compared to other estimation approaches. By contrast, the accuracy of conditional precision matrix estimations does not reach justifiable levels with any of the evaluated methods.

5 Empirical Applications

We consider the application of the proposed Bayesian nonparanormal conditional estimation to both foreign stock price indices and the blue chip stocks selected based on the market capitalization[4] within S&P 500 index. The first application concerning foreign stock price indices aims to estimate their interdependencies by examining conditional partial correlations. While conditional correlations are commonly employed for this purpose, they may conflate the effects of widespread global phenomena with those of specific, bilateral interactions. Conditional partial correlations are applied here with the aim of to mitigate the effect of common factors. In the second application, we test $\mathbb{H}_0 : \alpha_i = 0$ for $i = 1, 2, \ldots, N$ to validate if the excess return of a financial asset equals its factor loadings times the excess returns of related risk factors, plus a random component, in a frictionless market. Validating this hypothesis requires the estimation of precision matrices that are integral to Wald-type test statistics in the context of asset pricing models. We consider the $\hat{J}_\alpha$ test developed by Pesaran and Yamagata (2023), the GOS test by Gagliardini, Ossola, and Scaillet (2016), and the Standardized Wald tests based on the conditional precision matrices estimated by our proposed method and the DCC-NL. In applying our proposed method, we implement 4,000 iterations, including a 2,000-iteration burn-in period. The daily return for security i on day t, expressed as r_{it}, is computed as $r_{it} = 100 \log(p_t/p_{t-1})$, where p_t represents the closing price of the financial security on the given day.

5.1 Foreign Stock Price Indexes

In the application to the foreign stock price indexes, we analyze a combined time series from a chosen dataset of stock price indices, including the Dow Jones and NASDAQ from the United States, the DAX from Germany, the CAC40 from France, and the NIKKEI from Japan ($N = 5$). Our analysis covers 7,600 trading days ($T = 7,600$), stretching from January 4, 1991, to August 31, 2023. The data, which was obtained from Google Finance, ensures uniformity in the sample size, counteracting the variations in trading days across the indices. These variations result from national holidays, time zone differences, and market-specific practices.[5]

We apply our proposed Bayesian estimation approach to calculate the posterior mean of

[4]The market capitalization is calculated by multiplying the share price of the company's stock by the total number of its (outstanding) shares daily. Then, we take an average across the sample periods to rank the stocks based on the average market capitalization. From September 2, 2016, to July 31, 2023, most of the stocks in the list in Appendix C have been part of S&P 500 index.

[5]In our study, we focus on only 5 foreign stock indices. While this number may seem limited in high-dimensional settings, our main objective is to examine pairwise partial correlations. Given that there are 10 ($= N(N-1)/2$) such pairwise correlations when $N = 5$, a smaller set of variables is preferable for demonstrating the overall dependence across different time periods. This small number of variables allows for a clearer and more focused examination of the interrelationships among the selected stock indices.

conditional partial correlations, $\hat{\mathbf{\Psi}}_t$, as defined in Equation (2.8), using residuals from return regression without considering common factors as in (2.1). In contrast, for the conditional correlations, $\hat{\mathbf{R}}_t$, we employ the method proposed by Engle, Ledoit, and Wolf (2019), estimated using residuals from return regressions that include K common factors, estimated by principal component analysis (PCA). The number of factors is set at $K = 1$, by following Hallin and Liška (2007).

In this application, the conditional correlations and conditional partial correlations assess distinct aspects of the interdependence of the variables. Specifically, conditional correlations, derived from the residuals of a PCA regression, reflect the relationships between variables by adjusting for the variance captured by broad, statistically derived (unknown) common factors. This method shows the co-movement of variables in response to these overarching factors. However, it might not capture the direct connections between individual variables when all variables are considered. In contrast, conditional partial correlations with our proposed method offer a different perspective. They calculate the exclusive, bilateral relationships between variables, excluding the influence of any other variable in the dataset. This method distinctly determines the direct relationship between any two variables, irrespective of their categorization as common factors. Thus, while conditional correlations provide valuable context on how variables interact in light of PCA-based common factors, conditional partial correlations reveal the inherent associations between individual variable pairs, irrespective of the influence of other variables. Consequently, examining both conditional partial correlations and conditional correlations is beneficial, even when common factors are considered in the conditional correlations.

Table 7 provides summary statistics of $\hat{\mathbf{R}}_t = (\hat{r}_t(i,j))$, and $\hat{\mathbf{\Psi}}_t = (\hat{\psi}_t(i,j))$, across different stock index pairs for the period from April 1, 1991, to August 31, 2023. $\hat{r}_t(\text{DJI}, \text{NASDAQ})$ is positive with a mean of 0.47 and a standard deviation of 0.22, indicating moderate variability around a generally strong relationship. Similarly, $\hat{r}_t(\text{DAX}, \text{CAC40})$ shows a mean correlation of 0.42 and a conditional partial correlation mean of 0.24. These figures are among the highest in the dataset, indicating a robust linkage. The relatively stronger relations in both correlations and partial correlations for these index pairs could stem from several factors. The DJI and NASDAQ, both US stock indices, are more likely influenced by similar economic and market forces, resulting in a stronger correlation. The DAX and CAC40, representing major European economies, exhibit a strong relationship due to their geographical proximity and economic ties within the European Union, which could lead to synchronized economic cycles and business environments. The significant partial correlations suggest that even when controlling for other influences, the direct relationship between these European indices remains robust, likely due to shared economic policies, trade relationships, and financial regulations within the European market.

Table 8 presents the average values and standard deviations for the estimated conditional

Table 7: Descriptive Statistics of $\hat{\mathbf{R}}_t$ and $\hat{\mathbf{\Psi}}_t$: Full Sample Periods (01. 04. 1991 – 08. 31. 2023)

	$\hat{\mathbf{R}}_t$		$\hat{\mathbf{\Psi}}_t$	
Full sample periods (01.04.91–08.31.23)	Mean	Std	Mean	Std
DJI & NASDAQ	0.47	0.22	0.20	0.08
DJI & DAX	–0.46	0.16	0.06	0.07
DJI & CAC40	–0.44	0.16	0.07	0.07
DJI & NIKKEI	–0.31	0.14	0.01	0.08
NASDAQ & DAX	–0.60	0.12	0.06	0.07
NASDAQ & CAC40	–0.64	0.12	0.04	0.07
NASDAQ & NIKKEI	–0.31	0.13	0.02	0.08
DAX & CAC40	0.42	0.22	0.24	0.07
DAX & NIKKEI	–0.25	0.16	0.04	0.08
CAC40 & NIKKEI	–0.20	0.15	0.04	0.08

Notes: The table presents the average and standard deviations for estimated conditional correlations ($\hat{\mathbf{R}}_t$) and conditional partial correlations ($\hat{\mathbf{\Psi}}_t$). We derive $\hat{\mathbf{R}}_t$ using the approach proposed by Engle, Ledoit, and Wolf (2019) and obtain $\hat{\mathbf{\Psi}}_t$ through a Bayesian nonparanormal conditional estimation method we suggest. We calculate $\hat{\mathbf{R}}_t$ after adjusting for a single factor, identified via principal component analysis. Hallin and Liška (2007) method determines the number of factors to consider. The abbreviations for the stock indexes are as follows: DJI denotes the Dow Jones Industrial Average, NASDAQ signifies the National Association of Securities Dealers Automated Quotations, DAX stands for Deutscher Aktienindex, CAC40 is an acronym for Cotation AssistÃ©e en Continu 40, and NIKKEI represents the Nikkei 225 Stock Average.

correlations and the estimated conditional partial correlations across six distinct episodes of market turmoil: (1) the Asian Financial Crisis (July 1997 – December 1999), (2) the Dot-com Bubble Burst (March 2000 – October 2002), (3) the Great Recession (December 2007 – June 2009), (4) the European Sovereign Debt Crisis (October 2010 – August 2012), (5) the COVID–19 Pandemic (January 2022–August 2022), and (6) the FED's Inflation-Containment Rate Hikes (March 2022 – August 2023). The data estimates show that the mean of the conditional correlations for select index pairs diminishes or becomes increasingly negative amid market distress. For instance, the average conditional correlation between the DJI and NASDAQ indices fluctuates from 0.47 over the entire sample to –0.54 to 0.69 throughout the various crises, signaling a sizable conditional correlation during market instability compared to more stable periods. Furthermore, the standard deviations for the conditional correlations tend to be lower during crises than the sample period overall, suggesting a more uniform relationship between the indices in times of market stress, possibly due to a unified response to global financial shocks.

In examining the conditional partial correlations, their average values tend to decrease during market disruptions. For instance, the average values typically range from 0.01 to 0.25, but they frequently fall towards the lower end of this range or even to 0.00, particularly the DJI and NIKKEI pair during the Federal Reserve's rate hikes. Such decreases in average values suggest a reduction in the direct linkage between indices when considering other market influences.

Table 8: Descriptive Statistics of the conditional correlations and conditional partial correlations: Six Market disruption periods

	Conditional correlations		Conditional partial correlations	
Market disruption periods:	Mean	Std	Mean	Std
(1) Asian Financial Crisis (07.97 – 12.99)				
DJI & NIKKEI	–0.23	0.15	0.02	0.08
DAX & NIKKEI	–0.26	0.13	0.03	0.08
(2) The Dot-com Bubble Burst (03.20 – 10.02)				
DJI & NASDAQ	0.37	0.22	0.18	0.08
NASDAQ & DAX	–0.54	0.13	0.05	0.07
(3) The Great Recession (12.07 – 06.09)				
DJI & NASDAQ	0.69	0.09	0.23	0.07
DJI & NIKKEI	–0.42	0.09	0.01	0.08
(4) European Sovereign Debt Crisis (10.10 – 08.12)				
DJI & CAC40	–0.42	0.14	0.10	0.06
DAX & CAC40	0.39	0.11	0.25	0.07
(5) COVID–19 (01.22 – 08.22)				
Negative pairwise indices	–0.41	0.15	0.05	0.07
Positive pairwise indices	0.46	0.19	0.22	0.08
(6) FED's Inf.-Containment Rate Hikes (03.22 – 08.23)				
DJI & NASDAQ	0.45	0.13	0.22	0.07
DJI & NIKKEI	–0.29	0.11	0.00	0.08

Notes: The table presents the average and standard deviations for estimated conditional correlations ($\hat{\mathbf{R}}_t$) and conditional partial correlations ($\hat{\mathbf{\Psi}}_t$). We derive $\hat{\mathbf{R}}_t$ using the approach proposed by Engle, Ledoit, and Wolf (2019) and obtain $\hat{\mathbf{\Psi}}_t$ through a Bayesian nonparanormal conditional estimation method we suggest. We calculate $\hat{\mathbf{R}}_t$ after adjusting for a single factor, identified via principal component analysis. Hallin and Liška (2007) method determines the number of factors to consider. COVID-19 case shows the collected results of the negative and positive pairwise indices, where 'Negative pairwise indices' = {DJI & DAX', DJI & CAC40, DJI & NIKKEI, NASDAQ & DAX, NASDAQ & CAC40, NASDAQ & NIKKEI, DAX & NIKKEI, CAC40 & NIKKEI}, and 'Positve pairwise indices' = {DJI & NASDAQ, DAX & CAC40}. The abbreviations for the stock indexes are as follows: DJI denotes the Dow Jones Industrial Average, NASDAQ signifies the National Association of Securities Dealers Automated Quotations, DAX stands for Deutscher Aktienindex, CAC40 is an acronym for Cotation AssistÃ©e en Continu 40, and NIKKEI represents the Nikkei 225 Stock Average.

During these market disruption periods, the partial correlations' variances are generally similar to, or slightly lower than, those in the whole sample periods. For instance, the standard deviation for the conditional partial correlation between DJI and CAC40 drops to 0.06 in the period of the Great Recession from a previous value of 0.07, potentially indicating the same stable direct relationship despite the market fluctuations.

Our analysis indicates that in times of market upheaval, the relationships between indices, as captured by both conditional correlations and partial correlations, are characterized by lower average values but the same variances. This indicates a more uniform response to stress in the markets.

Figure 1 displays the estimated conditional correlations and conditional partial correlations

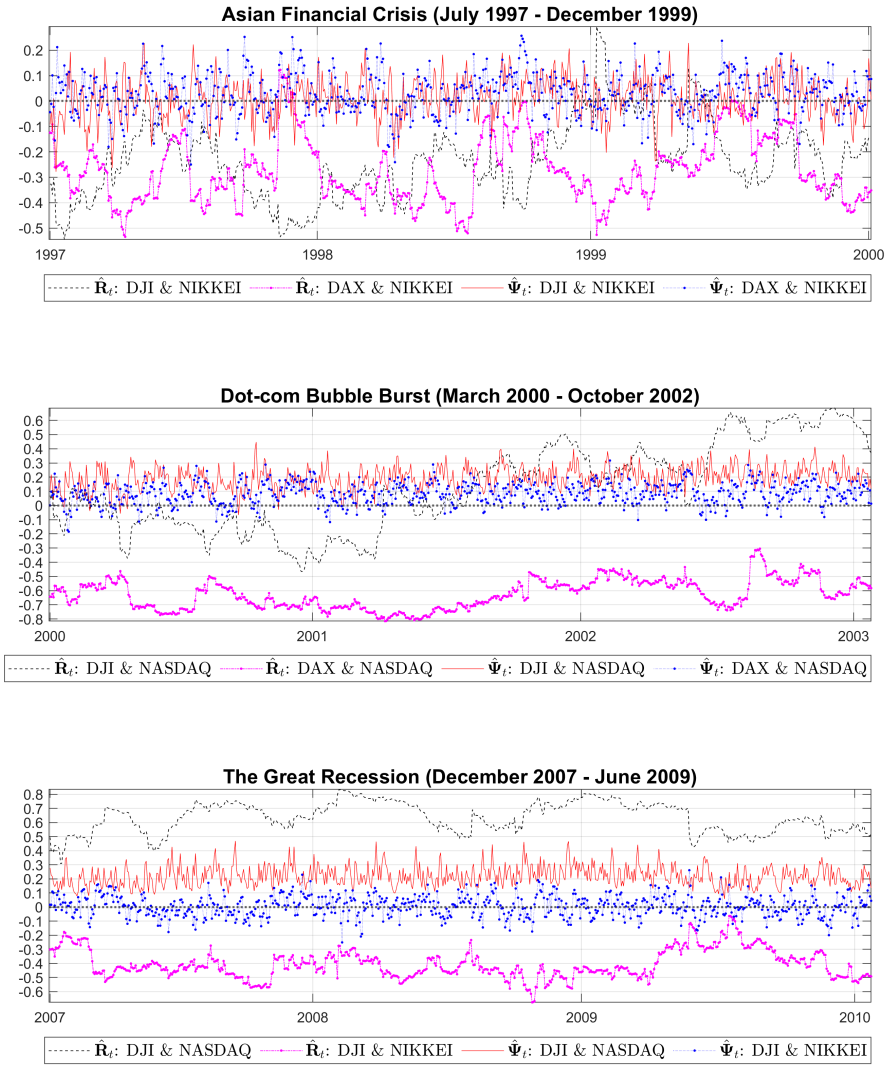

Figure 1: Conditional (Partial) Correlations in Market Disruption Periods: 1997 – 2009

Notes: The figure depicts the estimated conditional correlations ($\hat{\mathbf{R}}_t$) and conditional partial correlations ($\hat{\mathbf{\Psi}}_t$) during periods of market disruption, specifically throughout the Asian Financial Crisis, the Dot-com Bubble Burst, and the Great Recession. We derive $\hat{\mathbf{R}}_t$ using the approach proposed by Engle, Ledoit, and Wolf (2019) and obtain $\hat{\mathbf{\Psi}}_t$ through a Bayesian nonparanormal conditional estimation method we suggest. We calculate $\hat{\mathbf{R}}_t$ after adjusting for a single factor, identified via principal component analysis. Hallin and Liška (2007) method determines the number of factors to consider. The abbreviations for the stock indexes are as follows: DJI denotes the Dow Jones Industrial Average, NASDAQ signifies the National Association of Securities Dealers Automated Quotations, DAX stands for Deutscher Aktienindex, CAC40 is an acronym for Cotation AssistÃ©e en Continu 40, and NIKKEI represents the Nikkei 225 Stock Average.

for pairs of stock indices during three major market crises: the Asian Financial Crisis (1997-1999), the Dot-com Bubble Burst (2000-2002), and the Great Recession (2007-2009). The estimated mean, and variance values shown in this figure correspond to those listed in Table 8.

During the Asian Financial Crisis, the plot reveals fluctuations in the conditional correlations between the DJI and the NIKKEI, and between the DAX and NIKKEI, alongside their conditional partial correlations. The conditional correlations and partial correlations between DJI and NIKKEI and DAX and NIKKEI show different magnitudes. Specifically, DJI and NIKKEI's overall mean conditional correlation is -0.31 with a standard deviation of 0.14, as compared to -0.23 and 0.15, respectively, during the crisis. Conversely, DAX and NIKKEI maintain a stable mean conditional correlation, moving from -0.25 overall to -0.26 during the crisis with a reduced standard deviation from 0.16 to 0.13. This indicates that the relationship between DJI and NIKKEI exhibits a slight change during the crisis, whereas DAX and NIKKEI's relationship remained largely unchanged. The conditional partial correlations capture this nuanced difference; the DJI and NIKKEI pair show a minor increase in mean from 0.01 to 0.02, and the DAX and NIKKEI pair see a decrease from 0.04 to 0.03, with both pairs maintaining a standard deviation of 0.08.

As shown in the second subgraph, during the Dot-com Bubble Burst, the divergence between the $\hat{r}_t$ and $\hat{\psi}_t$ of DJI and NASDAQ and DAX and NASDAQ suggests differentiated market dynamics. This shift influenced the conditional correlation in investor preference from technology stocks to traditional "brick and mortar" stocks. Therefore, the negative swing in $\hat{r}_t(\text{DJI}, \text{NASDAQ})$ pre-mid-2001, which contrasts with the general positivity in $\hat{\mathbf{\Psi}}_t$ throughout the period, might indicate that while the tech and traditional sectors moved divergently in the market disruption, the inherent relationship between them, when isolated from the influence of the DAX and other indices (as the conditional partial correlation suggest), uniformly positive. The smaller magnitude of the conditional partial correlation could be due to the unique characteristics of the NASDAQ, which is heavily weighted towards technology stocks, which experienced a distinct reaction to the economic environment compared to the more diversified DJI and the European-focused DAX.

The Great Recession period also depicts the divergence in the conditional correlations and conditional partial correlations, particularly between DJI and NASDAQ, and DJI and NIKKEI. This divergence suggests the increased disconnections during the recession, reflecting varying degrees of integration and response to economic stress among different markets. The observed divergence in $\hat{r}_t(\text{DJI}, \text{NIKKEI})$ and $\hat{\psi}_t(\text{DJI}, \text{NIKKEI})$ during the Great Recession reflects the distinct economic environments and market responses in the United States and Japan. Geographical separation may contribute to market differentiation, with each country's unique fiscal and monetary policies, investor sentiment, and economic conditions influencing the markets, especially during the market disruption period. These factors lead to the distinct behavior of the indices, which is captured by partial correlations close to zero, revealing a disconnection not apparent in the conditional correlation. By contrast, the consistently positive relationship between DJI and NASDAQ, even after isolating other effects, underscores the significant in-

terdependence within the U.S. markets, which the conditional correlation also cannot capture. Therefore, the conditional partial correlation offers a granular perspective, capturing the underlying market relationships that conditional correlation might not fully disclose, revealing the unique market dynamics during the Great Recession.

Figure 2 presents the time-series behavior of the estimated conditional correlations and conditional partial correlations for stock index pairs during three significant market disruptions: (4) the European Sovereign Debt Crisis (October 2010 – August 2012), (5) the COVID–19 Pandemic (January 2022–August 2022), and (6) the FED's Inflation-Containment Rate Hikes (March 2022 – August 2023). These estimates of mean and variance correspond to the values tabulated in Table 8.

During the European Sovereign Debt Crisis, the $\hat{\mathbf{R}}_t$ between the DAX and CAC40 indices declined, indicating market segmentation within Euro, even though France and Germany avoided the worst of the crisis. This segmentation is discernible through reduced conditional correlations, yet the underlying connection between these two key Eurozone players remains inherently positive, as suggested by the $\hat{\mathbf{\Psi}}_t$. Conversely, the relationship between the DJI and CAC40 reflects higher volatility and a tendency towards a negative correlation in terms of $\hat{\mathbf{R}}_t$, which may stem from the disparate nature of the U.S. and French markets during market turbulence. This implies that the interactions between the DJI and CAC40 are more significantly influenced by extraneous indices rather than a direct financial linkage, underlining the divergent market behaviors under stress conditions between different economies.

During the COVID-19 pandemic, we analyze distinct groups of stock index pairs, categorized by positive and negative conditional correlations. Positive conditional correlations are consistently found between indices from the same country, like DJI and NASDAQ, or those belonging to the same economic area, such as DAX and CAC40 in the European Union. This indicates that indices within national or regional boundaries tend to move together, likely influenced by common economic conditions or collective investor sentiment. In contrast, negative conditional correlations between international index pairs suggest a disconnection of these markets during the pandemic. Additionally, the conditional partial correlations for these negatively correlated pairs are close to zero, indicating that their negative correlations are mostly driven by variables other than the direct relationship between the indices. When these variables are accounted for, the conditional partial correlation between these international indices is minimal, pointing to a fundamental disconnection during the pandemic. Thus, while local and regional markets showed some cohesion during the pandemic, the interconnectedness across global markets was disrupted.

During the Federal Reserve interest rate hikes aimed at containing inflation, the DJI and NASDAQ, both US indices, exhibited a similar positive conditional correlation, reflecting their representativeness of the US market despite the differences in sector composition within each

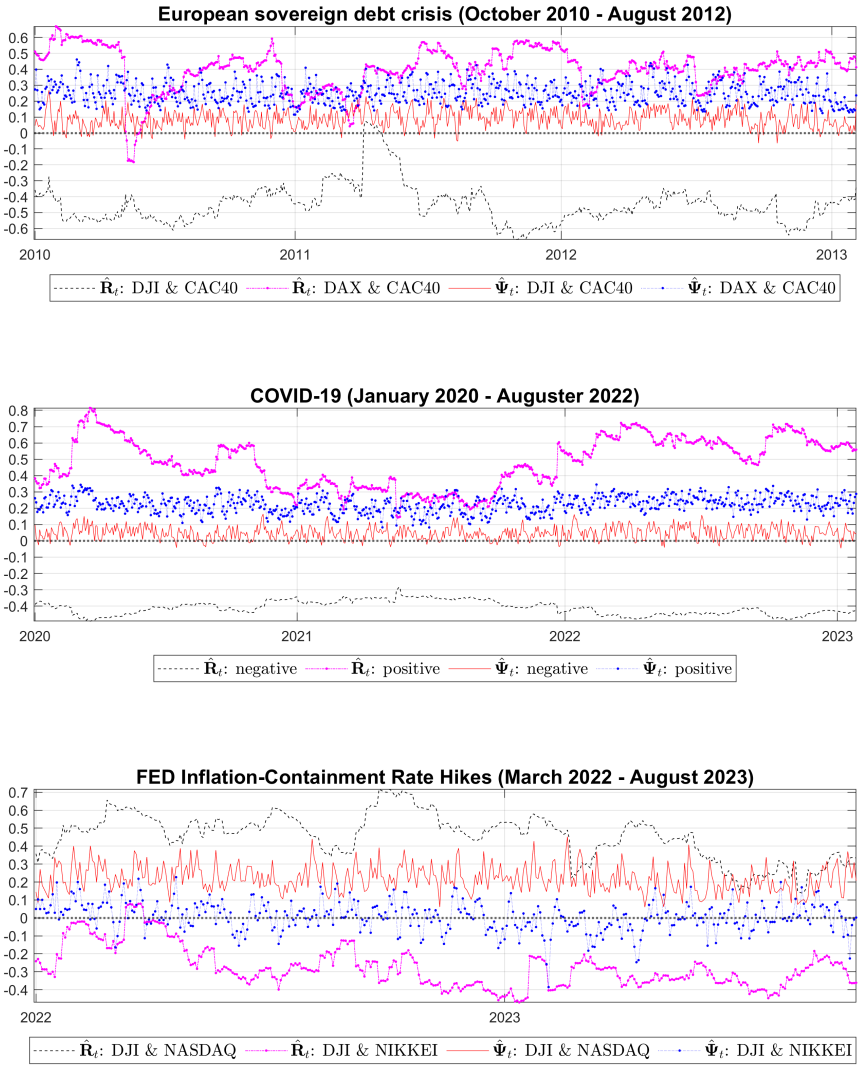

Figure 2: Conditional (Partial) Correlations in Market Disruption Periods: 2010 – 2023

Notes: The figure depicts the estimated conditional correlations ($\hat{\mathbf{R}}_t$) and conditional partial correlations ($\hat{\mathbf{\Psi}}_t$) during episodes of market turmoil, including the European sovereign debt crisis, the COVID-19 pandemic, and the Federal Reserve's rate hikes aimed at controlling inflation. We derive $\hat{\mathbf{R}}_t$ using the approach proposed by Engle, Ledoit, and Wolf (2019) and obtain $\hat{\mathbf{\Psi}}_t$ through a Bayesian nonparanormal conditional estimation method we suggest. We calculate $\hat{\mathbf{R}}_t$ after adjusting for a single factor, identified via principal component analysis. Hallin and Liška (2007) method determines the number of factors to consider. COVID-19 case shows the collected results of the negative and positive pairwise indices, where 'Negative pairwise indices' = {DJI & DAX', DJI & CAC40, DJI & NIKKEI, NASDAQ & DAX, NASDAQ & CAC40, NASDAQ & NIKKEI, DAX & NIKKEI, CAC40 & NIKKEI}, and 'Positive pairwise indices' = {DJI & NASDAQ, DAX & CAC40}. The abbreviations for the stock indexes are as follows: DJI denotes the Dow Jones Industrial Average, NASDAQ signifies the National Association of Securities Dealers Automated Quotations, DAX stands for Deutscher Aktienindex, CAC40 is an acronym for Cotation AssistÃ©e en Continu 40, and NIKKEI represents the Nikkei 225 Stock Average.

index. This similarity in movement contrasts with the period of the Dot-com Bubble, where sector rotation was a prominent feature. By contrast, $\hat{\psi}_t(\text{DJI}, \text{NIKKEI})$ is not statistically significant at the 1% level, suggesting a lack of meaningful linkage in their movements during this period. This lack of correlation could be attributed to the divergence in monetary policy approaches between the US and Japan. Specifically, Japan has not mirrored the US's interest rate increases, possibly signaling conditional dependence in their monetary policy stances. The conditional correlation, however, only presents a negative association rather than capturing the nuances of independent monetary policy decisions. This difference may imply the importance of distinguishing between correlation and causation: while the indices may move in opposite directions, it does not necessarily reflect a direct linkage to monetary policy.

Appendix B contains the ten plots detailing both conditional correlations and conditional partial correlations for the selected five foreign stock indices and their corresponding volatilities.

5.2 Daily Returns on Securities Selected from S&P 500

In this application, we consider a panel of 98 US blue chip stocks, well-established, financially sound companies recognized for their stability and reliability, across different industry sectors selected from S&P 500 based on the market capitalization.[6] The analysis covers the period from September 2, 2016, to July 31, 2023, encompassing 1,723 trading days. The data for this period is collected from Google and Yahoo Finance, and all companies included are constituents of S&P 500 index throughout this time frame.[7]

We obtained our time series data for the safe return rate and the five Fama-French factors from the data library of Ken French. For the risk-free rate(r_{ft}), we selected the one-month U.S. treasury bill rate. The market return (r_{mt}) is represented by the return on S&P 500 index, which includes the blue chip stocks in our study. Our analysis encompasses two model specifications assessed using three test statistics. The first is the capital asset pricing model (CAPM), and the second is the Fama and French (2015) five-factor model (FF5). The FF5 model is given by the equation:

$$r_{it} - r_{ft} = \hat{\alpha}_i + \hat{\beta}_{1,i}\text{MktRF}_t + \hat{\beta}_{2,i}\text{SMB}_t + \hat{\beta}_{3,i}\text{HML}_t + \hat{\beta}_{4,i}\text{RMW}_t + \hat{\beta}_{5,i}\text{CMA}_t + \hat{u}_{it}, \qquad (5.1)$$

[6]This study focuses on blue chip stocks for the analysis. It is important to recognize that such a selection may introduce a bias due to the inherent stability and reliability of these securities, potentially not reflecting the broader market dynamics. Furthermore, this approach might entail a survival bias, as it considers only well-performing stocks, excluding those that did not sustain or were more volatile. This limitation is noteworthy because investors, in practice, do not have the foresight to distinguish future 'blue chip' stocks from the entire market spectrum. Hence, the findings should be interpreted with caution, bearing in mind that they may not fully capture the investment decisions made under real-world uncertainty and the diverse nature of the market as represented by a broader index like S&P 500. See Appendix C for the full list of the companies.

[7]The analyses of both conditional correlations and conditional partial correlations, as discussed in Section 5.1, are also applicable to the current study. For a visual representation of these coefficients of firms from each GICS sector, refer to Appendix B, where detailed graphs are provided.

for $t = 1, 2, \ldots, 1723$ and $i = 1, 2, \ldots, 98$. We estimate equation (5.1) by using a rolling window of $h = 20$ trading days. In this model, MktRF_t is the market excess return defined as $r_{mt} - r_{ft}$, SMB_t represents the size premium measured by the difference in returns between small and large capitalization stock portfolios, HML_t captures the value premium through the difference in returns between high book-to-market and low book-to-market portfolios, RMW_t differentiates between the returns of firms with robust and weak profitability, and CMA_t contrasts the returns of firms with conservative and aggressive investment profiles.

Our application examines three test statistics: the $\hat{J}_\alpha$ test developed by Pesaran and Yamagata (2023), the GOS test by Gagliardini, Ossola, and Scaillet (2016), and the Standardized Wald test (SW). Pesaran and Yamagata (2023) demonstrate that the GOS and SW tests tend to falsely reject true null hypotheses, especially when the time dimension T, is smaller than the cross-sectional dimension N, compromising their effectiveness in both size and power.

For panel regressions based on time series data, we specify the model as

$$\mathbf{y}_{i\cdot} = \alpha_i \boldsymbol{\tau}_T + \mathbf{F}\boldsymbol{\beta}_i + \mathbf{u}_{i\cdot}, \tag{5.2}$$

where $\mathbf{y}_{i\cdot} = (y_{i1}, y_{i2}, \ldots, y_{iT})'$, $\mathbf{F}' = (\mathbf{f}_1, \mathbf{f}_2, \ldots, \mathbf{f}_T)$, and $\mathbf{u}_{i\cdot} = (u_{i1}, u_{i2}, \ldots, u_{iT})'$. We test the null hypothesis $\mathbb{H}_0 : \boldsymbol{\alpha} = \mathbf{0}$, by employing the SW test statistic, written as

$$\text{SW} = \frac{(\boldsymbol{\tau}_T' \mathbf{M}_F \boldsymbol{\tau}_T)\, \hat{\boldsymbol{\alpha}} \boldsymbol{\Sigma}_{\mathbf{u}}^{-1} \hat{\boldsymbol{\alpha}} - N}{\sqrt{2N}}, \tag{5.3}$$

where $\mathbf{M}_F = \mathbf{I}_T - \mathbf{F}(\mathbf{F}'\mathbf{F})^{-1}\mathbf{F}'$ and $\boldsymbol{\alpha} = (\alpha_1, \alpha_2, \ldots, \alpha_N)'$. The test procedure requires the estimation of $\boldsymbol{\Sigma}_{\mathbf{u}}^{-1}$, which is where our proposed estimators can be applied.

However, as noted above, the SW test suffers from size distortions when $T < N$ and is not designed for time-varying contexts, thus ruling out the use of rolling windows. To address this, we modify the SW test by substituting $\boldsymbol{\Sigma}_{\mathbf{u}}^{-1}$ with our proposed estimator for the conditional precision matrix, $\hat{\mathbf{P}}_{t,\mathbf{u}}$ in Equation (2.6). This is done by first conducting an ordinary least squares regression of (5.2) for each cross-sectional unit to obtain the residuals, which are then combined across all units to form $\hat{\mathbf{U}} = (\hat{\mathbf{u}}_{1\cdot}, \hat{\mathbf{u}}_{2\cdot}, \ldots, \hat{\mathbf{u}}_{N\cdot}) = (\hat{\mathbf{u}}_1, \hat{\mathbf{u}}_2 \ldots, \hat{\mathbf{u}}_T)'$, where $\hat{\mathbf{u}}_t = (u_{1t}, u_{2t}, \ldots, u_{Nt})'$. Applying our Bayesian estimation method to these residuals, we conduct the following time-dependent SW test, written as

$$\text{SW}\left(\hat{\mathbf{P}}_{t,\mathbf{u}}\right) = \frac{(\boldsymbol{\tau}_T' \mathbf{M}_F \boldsymbol{\tau}_T)\, \hat{\boldsymbol{\alpha}} \hat{\mathbf{P}}_{t,\mathbf{u}} \hat{\boldsymbol{\alpha}} - N}{\sqrt{2N}}, \tag{5.4}$$

which allows for the calculation of test statistics when $T > N$.

In addition to our Bayesian nonparanormal conditional estimator denoted by $\text{SW}(\hat{\mathbf{P}}_{t,\mathbf{u}})$, we also consider an alternative method for estimating the conditional precision matrix. This second

approach, based on the work of Engle, Ledoit, and Wolf (2019), utilizes the nonlinear shrinkage estimation of the conditional correlation matrices to obtain estimated conditional covariance matrix, $\hat{\mathbf{\Sigma}}_{t,\mathbf{u}}$, and is represented as SW($\hat{\mathbf{\Sigma}}_{t,\mathbf{u}}^{-1}$). Test statistics of $\hat{J}_\alpha$ and GOS are calculated using 20-day rolling windows for daily estimates, covering both the entire sample period and distinct periods of market disruption.[8] For SW tests, conditional precision matrices are determined for each $t = 1, 2, \ldots, T$, utilizing all T observations. Unlike the rolling window approach, the SW test statistic is calculated for each period t. Rejection frequencies for these test statistics are then computed at both 5% and 1% significance levels.

Table 9 summarizes the rejection frequencies of the $\hat{J}_\alpha$, GOS and SW$_t$ tests based on the CAPM and FF5 model, using the blue chip stocks from S&P 500 index at two nominal sizes (5% or 1%) during both the full sample period (09.02.16–07.31.23) and specific periods characterized by market disruption periods: (1) the Post-Crisis Int. Rate Normalization (12.02.16–06.28.19), (2) COVID-19 (01.20.20–08.31.22), and (3) the FED's Inf.-Containment Rate Hike (03.16.22–07.31.23) periods. The Post-Crisis Interest Rate Normalization period refers to the phase during which the Federal Reserve increased benchmark interest rates, moving away from the near-zero rates that were in place to support economic recovery after the 2008 financial crisis. This shift impacted asset valuations and introduced volatility as markets adjusted to a new interest rate regime. The onset of the COVID-19 global pandemic led to unprecedented economic turmoil, supply chain disruptions, and extreme market volatility, prompting a flight to safety among investors and significant intervention by central banks. Lastly, the Federal Reserve's Inflation-Containment Rate Hikes reflect a period during which the central bank implemented a series of interest rate increases to manage rising inflation, thereby increasing the cost of borrowing and affecting investor sentiment and market liquidity, thus contributing to further market instability.

In the case of the CAPM model, the $\hat{J}_\alpha$ test statistic shows rejection frequencies that range from 0.10 to 0.75 at the 0.05 significance level. During market disruption periods, the rejection frequencies are higher, suggesting that the CAPM model is less reliable during these periods. At the 0.01 significance level, the rejection frequencies are slightly lower but exhibit a similar pattern. The GOS test exhibits high rejection frequencies across all periods and significance levels, often reaching 0.99 or 1.00, which suggests a strong rejection of the null hypothesis and highlights potential inadequacies in the models tested, as shown in Pesaran and Yamagata (2023). For the FF5 model, the rejection rates are also high across all tests, especially during the post-crisis interest rate normalization period. This indicates that even a more comprehensive model like the FF5 model may struggle to explain asset returns during volatile periods.

The observed deviation in the rejection frequencies for $\hat{J}_\alpha$ during the COVID-19 pandemic may be attributed to a combination of factors, including the global scope and unprecedented

[8] In the literature, $\hat{J}_\alpha$ and GOS test statistics are calculated using monthly observations with 60-month windows. In contrast, our study calculates the test statistics of $\hat{J}_\alpha$ and GOS using daily observations with a 20-day rolling window.

Table 9: Rejection Frequencies of the $\hat{J}_\alpha$, GOS, and SW tests

Tests	$\hat{J}_\alpha$	GOS	SW($\hat{\mathbf{P}}_{t,\mathbf{u}}$)	SW($\hat{\mathbf{\Sigma}}^{-1}_{t,\mathbf{u}}$)
CAPM model				
Significance level of 0.05				
Full sample period (09.02.16–07.31.23)	0.49	0.96	0.60	0.63
Market disruption periods:				
(1) Post-Crisis Int. Rate Normalization (12.02.16–06.28.19)	0.75	0.99	0.34	1.00
(2) COVID-19 (01.20.20–08.31.22)	0.10	0.89	0.81	0.27
(3) FED's Inf.-Containment Rate Hikes (03.16.22–07.31.23)	0.70	0.99	0.89	0.24
Significance level of 0.01				
Full sample period (09.02.16–07.31.23)	0.43	0.94	0.49	0.58
Market disruption periods:				
(1) Post-Crisis Int. Rate Normalization (12.02.16–06.28.19)	0.67	0.98	0.24	1.00
(2) COVID-19 (01.20.20–08.31.22)	0.08	0.85	0.69	0.21
(3) FED's Inf.-Containment Rate Hikes (03.16.22–07.31.23)	0.66	0.98	0.79	0.10
FF5 model				
Significance level of 0.05				
Full sample period (09.02.16–07.31.23)	0.71	1.00	0.76	0.78
Market disruption periods:				
(1) Post-Crisis Int. Rate Normalization (12.02.16–06.28.19)	1.00	1.00	0.75	1.00
(2) COVID-19 (01.20.20–08.31.22)	0.23	0.99	0.80	0.68
(3) FED's Inf.-Containment Rate Hikes (03.16.22–07.31.23)	0.96	1.00	0.86	0.31
Significance level of 0.01				
Full sample period (09.02.16–07.31.23)	0.69	1.00	0.69	0.67
Market disruption periods:				
(1) Post-Crisis Int. Rate Normalization (12.02.16–06.28.19)	1.00	1.00	0.69	1.00
(2) COVID-19 (01.20.20–08.31.22)	0.19	0.99	0.72	0.51
(3) FED's Inf.-Containment Rate Hikes (03.16.22–07.31.23)	0.95	1.00	0.81	0.09

Notes: This table presents the rejection frequencies with the test statistics $\hat{J}_\alpha$, GOS, SW($\hat{\mathbf{P}}_{t,\mathbf{u}}$), and SW($\hat{\mathbf{\Sigma}}_{t,\mathbf{u}}$) of null hypotheses $\mathbb{H}_0 : \alpha_i = 0$ at significance levels of 0.05 and 0.01. The tests are carried out in the case of the capital asset pricing model (CAPM) and Fama-French five-factor (FF5) models to the securities within S&P 500 index. The test statistics of $\hat{J}_\alpha$ and GOS are computed using rolling windows of 20 days for daily estimates, spanning both the entire sample period and specific periods of market disruption. The SW($\hat{\mathbf{P}}_{t,\mathbf{u}}$) represents the standardized Wald test statistic computed with $\hat{\mathbf{P}}_{t,\mathbf{u}}$, obtained through Bayesian nonparanormal conditional estimation. SW($\hat{\mathbf{\Sigma}}_{t,\mathbf{u}}$) denotes the standardized Wald test statistic calculated using $\hat{\mathbf{\Sigma}}_{t,u}$, as estimated by the DCC–NL model Engle, Ledoit, and Wolf (2019).

nature of market disruptions during this time. The stabilizing actions by governments and interventions by central banks during this period might have contributed to a more predictable relationship between returns and identified risk factors, despite this relationship being nonlinear. Additionally, the use of blue-chip stocks from S&P 500 in our analysis could introduce selection bias, potentially influencing these results. Furthermore, the difference in methodologies, where the $\hat{J}_\alpha$ test employs rolling windows and our proposed SW test calculates conditional precision matrices using the full sample for all $t = 1, 2, \ldots, T$, may also contribute to the observed discrepancies.

The comparative evaluation between the SW test and the $\hat{J}_\alpha$ test reveals that the SW($\hat{\mathbf{P}}_{t,\mathbf{u}}$) test yields rejection frequencies that are aligned with those from the $\hat{J}_\alpha$ test throughout the overall sample periods. However, during periods of market disruptions, especially those coinciding with the COVID-19 pandemic, both tests exhibit distinct variations in rejection frequencies, indicating that they may respond differently to market distress.

6 Conclusions

This paper makes two main contributions to the literature on high-dimensional multivariate volatility modeling, focusing on the estimation of conditional precision matrices and the exploration of conditional dependence.

Our first contribution is the development of a Bayesian method for estimating conditional precision matrices within a high-dimensional DCC-MGARCH framework. This method circumvents the need to invert conditional covariance matrices, which is typically challenging due to semi-positive definiteness. Our Bayesian approach, leveraging the Wishart distribution, simplifies this process. The estimation utilizes the Metropolis-Hastings algorithm within Gibbs sampling. To estimate the unconditional precision matrix, we employ a horseshoe prior, introducing sparsity in high-dimensional contexts.

The second contribution is providing estimates of conditional precision and partial correlation matrices, crucial for understanding volatility interconnections. This is achieved through a Bayesian nonparanormal framework, which utilizes rank transformation to convert non-Gaussian distributions into approximate Gaussian ones. Additionally, by implementing a univariate GARCH model for each security, we derive the conditional precision matrix from the conditional inverse correlation matrix, an approach that outperforms standard nonparanormal rank-transformation methods in identifying the precision matrix.

We validate our approach through Monte Carlo simulations, comparing it with existing methods, and find our Bayesian estimator to be more effective in the simulation designs, particularly in estimating conditional precision and correlation matrices. Applying our method to empirical data, we analyze daily foreign stock price indices and returns on blue chip stocks from S&P 500.

Future research is encouraged to extend the current framework by incorporating variational inference instead of the MCMC approach to improve the computational aspect and the development of conditional tail dependence to improve partial correlation. Such extensions would build upon the foundational work presented here and offer new avenues for capturing more complex dependencies and behaviors in financial markets.

References

Aas, K., C. Czado, A. Frigessi, and H. Bakken (2009): "Pair-copula constructions of multiple dependence," *Insurance: Mathematics and economics*, 44(2), 182–198.

Anatolyev, S., and V. Pyrlik (2022): "Copula shrinkage and portfolio allocation in ultra-high dimensions," *Journal of Economic Dynamics and Control*, 143, 104508.

Ardia, D. (2008): "Bayesian estimation of the GARCH (1, 1) model with normal innovations," *Financial Risk Management with Bayesian Estimation of GARCH Models: Theory and Applications*, pp. 17–37.

Asai, M., and M. McAleer (2009): "The structure of dynamic correlations in multivariate stochastic volatility models," *Journal of Econometrics*, 150(2), 182–192.

Bailey, N., M. H. Pesaran, and L. V. Smith (2019): "A multiple testing approach to the regularisation of large sample correlation matrices," *Journal of Econometrics*, 208(2), 507–534.

Baillie, R. T., T. Bollerslev, and H. O. Mikkelsen (1996): "Fractionally integrated generalized autoregressive conditional heteroskedasticity," *Journal of econometrics*, 74(1), 3–30.

Barigozzi, M., and C. Brownlees (2019): "Nets: Network estimation for time series," *Journal of Applied Econometrics*, 34(3), 347–364.

Bauwens, L., and S. Laurent (2005): "A new class of multivariate skew densities, with application to generalized autoregressive conditional heteroscedasticity models," *Journal of Business & Economic Statistics*, 23(3), 346–354.

Bhattacharya, A., A. Chakraborty, and B. K. Mallick (2016): "Fast sampling with Gaussian scale mixture priors in high-dimensional regression," *Biometrika*, p. asw042.

Bickel, P. J., and E. Levina (2008): "Covariance regularization by thresholding," *The Annals of Statistics*, 36(6), 2577–2604.

Billio, M., M. Caporin, and M. Gobbo (2003): "Block dynamic conditional correlation multivariate GARCH models," *Università di Venezia*.

Bollerslev, T. (1986): "Generalized autoregressive conditional heteroskedasticity," *Journal of econometrics*, 31(3), 307–327.

Cai, T., and W. Liu (2011): "Adaptive thresholding for sparse covariance matrix estimation," *Journal of the American Statistical Association*, 106(494), 672–684.

Chen, C. W., F.-C. Liu, and M. K. So (2008): "Heavy-tailed-distributed threshold stochastic volatility models in financial time series," *Australian & New Zealand Journal of Statistics*, 50(1), 29–51.

Chen, C. W., and M. K. So (2006): "On a threshold heteroscedastic model," *International Journal of Forecasting*, 22(1), 73–89.

Chen, J., D. Li, and O. Linton (2019): "A new semiparametric estimation approach for large dynamic covariance matrices with multiple conditioning variables," *Journal of Econometrics*, 212(1), 155–176.

Chen, Z., and C. Leng (2016): "Dynamic covariance models," *Journal of the American Statistical*

Association, 111(515), 1196–1207.

De Nard, G., O. Ledoit, and M. Wolf (2021): "Factor models for portfolio selection in large dimensions: The good, the better and the ugly," *Journal of Financial Econometrics*, 19(2), 236–257.

Dobra, A., and A. Lenkoski (2011): "Copula Gaussian graphical models and their application to modeling functional disability data," *The Annals of Applied Statistics*, 5(2A), 969 – 993.

Engle, R. F. (1982): "Autoregressive conditional heteroscedasticity with estimates of the variance of United Kingdom inflation," *Econometrica: Journal of the econometric society*, pp. 987–1007.

——— (2002): "Dynamic Conditional Correlation: A Simple Class of Multivariate Generalized Autoregressive Conditional Heteroskedasticity Models," *Journal of Business & Economic Statistics*, 20(3), 339–350.

Engle, R. F., O. Ledoit, and M. Wolf (2019): "Large Dynamic Covariance Matrices," *Journal of Business & Economic Statistics*, 37(2), 363–375.

Fan, J., Y. Liao, and M. Mincheva (2013): "Large covariance estimation by thresholding principal orthogonal complements," *Journal of the Royal Statistical Society Series B: Statistical Methodology*, 75(4), 603–680.

Fan, J., J. Zhang, and K. Yu (2012): "Vast portfolio selection with gross-exposure constraints," *Journal of the American Statistical Association*, 107(498), 592–606.

Fernández, C., and M. F. Steel (1998): "On Bayesian modeling of fat tails and skewness," *Journal of the American Statistical Association*, 93(441), 359–371.

Fioruci, J. A., R. S. Ehlers, and M. G. Andrade Filho (2014): "Bayesian multivariate GARCH models with dynamic correlations and asymmetric error distributions," *Journal of Applied Statistics*, 41(2), 320–331.

Gagliardini, P., E. Ossola, and O. Scaillet (2016): "Time-varying risk premium in large cross-sectional equity data sets," *Econometrica*, 84(3), 985–1046.

Giannone, D., M. Lenza, and G. E. Primiceri (2021): "Economic predictions with big data: The illusion of sparsity," *Econometrica*, 89(5), 2409–2437.

Hallin, M., and R. Liška (2007): "Determining the number of factors in the general dynamic factor model," *Journal of the American Statistical Association*, 102(478), 603–617.

Hoff, P. D. (2007): "Extending the rank likelihood for semiparametric copula estimation," *The Annals of Applied Statistics*, 1(1), 265 – 283.

Kim, J.-M., and H. Jung (2016): "Linear time-varying regression with Copula–DCC–GARCH models for volatility," *Economics Letters*, 145, 262–265.

Ledoit, O., and M. Wolf (2003): "Improved estimation of the covariance matrix of stock returns with an application to portfolio selection," *Journal of Empirical Finance*, 10(5), 603–621.

——— (2004a): "Honey, I shrunk the sample covariance matrix," *Jounral of Portfolio Management*, (30), 110–119.

——— (2004b): "A well-conditioned estimator for large-dimensional covariance matrices," *Journal of Multivariate Analysis*, 88(2), 365–411.

——— (2012): "Nonlinear shrinkage estimation of large-dimensional covariance matrices," *The An-*

nals of Statistics, 40(2), 1024–1060.

——— (2017): "Nonlinear Shrinkage of the Covariance Matrix for Portfolio Selection: Markowitz Meets Goldilocks," *The Review of Financial Studies*, 30(12), 4349–4388.

——— (2020): "Analytical nonlinear shrinkage of large-dimensional covariance matrices," *The Annals of Statistics*, 48(5), 3043–3065.

——— (2022): "Quadratic shrinkage for large covariance matrices," *Bernoulli*, 28(3), 1519–1547.

Li, Z. R., and T. H. McCormick (2019): "An expectation conditional maximization approach for Gaussian graphical models," *Journal of Computational and Graphical Statistics*, 28(4), 767–777.

Liu, H., F. Han, M. Yuan, J. Lafferty, and L. Wasserman (2012): "High-dimensional semiparametric Gaussian copula graphical models," *The Annals of Statistics*, 40(4), 2293 – 2326.

Liu, H., J. Lafferty, and L. Wasserman (2009): "The nonparanormal: Semiparametric estimation of high dimensional undirected graphs," *Journal of Machine Learning Research*, 10(10).

Mohammadi, A., F. Abegaz, E. Heuvel, and E. C. Wit (2017): "Bayesian modelling of Dupuytren disease by using Gaussian copula graphical models," *Journal of the Royal Statistical Society Series C: Applied Statistics*, 66(3), 629–645.

Mohammadi, A., and E. C. Wit (2015): "Bayesian Structure Learning in Sparse Gaussian Graphical Models," *Bayesian Analysis*, 10(1), 109 – 138.

Mulgrave, J. J., and S. Ghosal (2020): "Bayesian Inference in Nonparanormal Graphical Models," *Bayesian Analysis*, 15(2), 449 – 475.

——— (2022): "Regression-based Bayesian estimation and structure learning for nonparanormal graphical models," *Statistical Analysis and Data Mining: The ASA Data Science Journal*, 15(5), 611–629.

——— (2023): "Bayesian analysis of nonparanormal graphical models using rank-likelihood," *Journal of Statistical Planning and Inference*, 222, 195–208.

Müller, D., and C. Czado (2019a): "Dependence modelling in ultra high dimensions with vine copulas and the Graphical Lasso," *Computational Statistics & Data Analysis*, 137, 211–232.

——— (2019b): "Selection of sparse vine copulas in high dimensions with the lasso," *Statistics and Computing*, 29(2), 269–287.

Nard, G. D., R. F. Engle, O. Ledoit, and M. Wolf (2022): "Large dynamic covariance matrices: Enhancements based on intraday-data," *Journal of Banking & Finance*, 138, 106426.

Nelson, D. B. (1991): "Conditional heteroskedasticity in asset returns: A new approach," *Econometrica: Journal of the econometric society*, pp. 347–370.

Neville, S. E., J. T. Ormerod, and M. P. Wand (2014): "Mean field variational Bayes for continuous sparse signal shrinkage: Pitfalls and remedies," *Electronic Journal of Statistics*, 8(1), 1113 – 1151.

Oh, D. H., and A. J. Patton (2016): "High-dimensional copula-based distributions with mixed frequency data," *Journal of Econometrics*, 193(2), 349–366.

——— (2017): "Modeling dependence in high dimensions with factor copulas," *Journal of Business & Economic Statistics*, 35(1), 139–154.

——— (2023): "Dynamic factor copula models with estimated cluster assignments," *Journal of Econometrics*.

Pakel, C., N. Shephard, K. Sheppard, and R. F. Engle (2021): "Fitting Vast Dimensional Time-Varying Covariance Models," *Journal of Business & Economic Statistics*, 39(3), 652–668.

Patton, A. J. (2009): "Copula–based models for financial time series," in *Handbook of financial time series*, pp. 767–785. Springer.

Pesaran, M. H., and T. Yamagata (2023): "Testing for Alpha in Linear Factor Pricing Models with a Large Number of Securities," *Journal of Financial Econometrics*.

Pitt, M., D. Chan, and R. Kohn (2006): "Efficient Bayesian inference for Gaussian copula regression models," *Biometrika*, 93(3), 537–554.

Poignard, B., and M. Asai (2023): "High-dimensional sparse multivariate stochastic volatility models," *Journal of Time Series Analysis*, 44(1), 4–22.

Rothman, A. J., E. Levina, and J. Zhu (2009): "Generalized thresholding of large covariance matrices," *Journal of the American Statistical Association*, 104(485), 177–186.

Rue, H., and L. Held (2005): *Gaussian Markov random fields: theory and applications*. CRC press.

Sentana, E. (1995): "Quadratic ARCH models," *The Review of Economic Studies*, 62(4), 639–661.

——— (2009): "The econometrics of mean-variance efficiency tests: a survey," *The Econometrics Journal*, 12(3), C65–C101.

So, M. K., and I. W. Yip (2012): "Multivariate GARCH models with correlation clustering," *Journal of Forecasting*, 31(5), 443–468.

Tse, Y. K., and A. K. C. Tsui (2002): "A Multivariate Generalized Autoregressive Conditional Heteroscedasticity Model with Time-Varying Correlations," *Journal of Business & Economic Statistics*, 20(3), 351–362.

A Appendix

A.1 Algorithm 2: Sampling the transformed standardized residuals

Algorithm 2 Sample $\mathbf{Z} \sim \mathcal{N}(\mathbf{0}, \mathbf{S}^{-1})$

for i=1:n **do**
  for r=1:T **do**
    if $r = 1$ **then**
      $z_{i,t_0} = -\infty$
    else
      $z_{i,t_{r-1}} = u_{i,t_{r-1}}$
    end if
    if $r = T$ **then**
      $z_{i,t_{T+1}} = \infty$
    else
      $z_{i,t_{r+1}} = u_{i,t_{r+1}}$
    end if
    Compute $\mu_{t_r,i} = -\boldsymbol{\psi}_{i,i}^{-1} \boldsymbol{\Psi}_{n\setminus i,i} \mathbf{u}_{n\setminus i,t_r}$
    Compute $\sigma_i^2 = \boldsymbol{\psi}_{i,i}^{-1}$
    Sample $z_{i,t_r} \sim \mathcal{TN}(\mu_{t_r,i}, \sigma_i^2; z_{i,t_{r-1}} < z_{i,t_r} < z_{i,t_{r+1}})$
  end for
end for

A.2 Algorithm 3: Sampling the sparse unconditional precision matrix

Expanding upon the variation in the horseshoe prior specification, as articulated in Model III by Neville, Ormerod, and Wand (2014), and Mulgrave and Ghosal (2022, 2023) set forth a series of prior distributions for $\boldsymbol{\beta}$ in Equation (2.16). For $j = 1, 2, \ldots, N$ and $i = j+1, j+2, \ldots, N$, the priors are formulated as follows:

$$
\begin{aligned}
\mathbf{Z}_j | \mathbf{Z}_{i>j}, \boldsymbol{\beta}_{i>j} \sigma_j^2 &\sim \mathcal{N}\left(\mathbf{Z}_{i>j} \boldsymbol{\beta}_{i>j}, \sigma_j^2 \mathbb{I}\right), \\
\boldsymbol{\beta}_{i>j} | \lambda_j^2, \mathbf{b}_{i>j}, \sigma_j^2 &\sim \mathcal{N}\left(\mathbf{0}, \frac{\sigma_j^2 \mathbf{b}_{i>j} c^2 \lambda_j^2}{N^2 i}\right), \\
\lambda_j^2 | a_j &\sim \mathcal{IG}\left(\frac{1}{2}, \frac{1}{a_j}\right), \quad a_j \sim \mathcal{IG}\left(\frac{1}{2}, 1\right), \\
\mathbf{b}_{i>j} | h_{i>j} &\sim \mathcal{IG}\left(\frac{1}{2}, \frac{1}{h_{i>j}}\right), \quad h_{i>j} \sim \mathcal{IG}\left(\frac{1}{2}, 1\right), \\
\sigma_j^2 &\sim \mathcal{IG}\left(0.01, 0.01\right),
\end{aligned}
\tag{A.1}
$$

where $\mathcal{IG}$ stands for the inverse gamma distribution, and σ_j^2 is chosen to be a diffuse prior. Given these priors, the posterior distribution for $\boldsymbol{\beta}_{i>j}$ can be derived. The probability density in Equation (2.16) is:

$$\mathcal{L}\left(\mathbf{Z}_j|\mathbf{Z}_{i>j}\boldsymbol{\beta}_{i>j},\sigma_j^2\right) \propto \exp\left\{-\frac{1}{2\sigma_j^2}\left(\mathbf{Z}_j-\mathbf{Z}_{i>j}\boldsymbol{\beta}_{i>j}\right)'\left(\mathbf{Z}_j-\mathbf{Z}_{i>j}\boldsymbol{\beta}_{i>j}\right)\right\}. \tag{A.2}$$

Coupling this with the prior distribution for $\boldsymbol{\beta}_{i>j}$ in Equation (A.1), defined as:

$$p\left(\boldsymbol{\beta}_{i>j}|\lambda_j^2,\mathbf{b}_{i>j},\sigma_j^2\right) \propto \exp\left\{-\frac{N^2 i}{2\sigma_j^2\mathbf{b}_{i>j}c^2\lambda_j^2}\boldsymbol{\beta}_{i>j}'\boldsymbol{\beta}_{i>j}\right\}. \tag{A.3}$$

Then, from Equations (A.2) and (A.3), the resulting posterior distribution is:

$$\begin{aligned}
p\left(\boldsymbol{\beta}_{i>j}|\mathbf{Z}_j,\mathbf{Z}_{i>j},\lambda_j^2,b_{i>j},\sigma_j^2\right) &\propto \mathcal{L}\left(\mathbf{Z}_j|\mathbf{Z}_{i>j}\boldsymbol{\beta}_{i>j},\sigma_j^2\right)\cdot p\left(\boldsymbol{\beta}_{i>j}|\lambda_j^2,\mathbf{b}_{i>j},\sigma_j^2\right)\\
&\propto \exp\left\{-\frac{1}{2\sigma_j^2}\left(\mathbf{Z}_j-\mathbf{Z}_{i>j}\boldsymbol{\beta}_{i>j}\right)'\left(\mathbf{Z}_j-\mathbf{Z}_{i>j}\boldsymbol{\beta}_{i>j}\right)\right.\\
&\quad\left.-\frac{N^2 i}{2\sigma_j^2\mathbf{b}_{i>j}c^2\lambda_j^2}\boldsymbol{\beta}_{i>j}'\boldsymbol{\beta}_{i>j}\right\}\\
&\propto \exp\left\{-\frac{1}{2\sigma_j^2}\boldsymbol{\beta}_{i>j}'\left(\mathbf{Z}_{i>j}'\mathbf{Z}_{i>j}+\operatorname{diag}\left\{\frac{N^2 i}{2\sigma_j^2\mathbf{b}_{i>j}c^2\lambda_j^2}\right\}\right)\boldsymbol{\beta}_{i>j}\right.\\
&\quad\left.+\frac{1}{\sigma_j^2}\boldsymbol{\beta}_{i>j}'\mathbf{Z}_{i>j}'\mathbf{Z}_j\right\}.
\end{aligned}$$

The distribution exhibits Gaussian properties with mean mean $\mathbf{A}^{-1}\mathbf{Z}_{i>j}'\mathbf{Z}_j$ and covariance $\sigma_j^2\mathbf{A}^{-1}$, where $\mathbf{A}=\mathbf{Z}_{i>j}'\mathbf{Z}_{i>j}+\operatorname{diag}\left\{\frac{N^2 i}{2\sigma_j^2\mathbf{b}_{i>j}c^2\lambda_j^2}\right\}$ and we can write it as

$$\boldsymbol{\beta}_{i>j}|\lambda_j^2,\mathbf{b}_{i>j},\sigma_j^2 \sim \mathcal{N}\left(\mathbf{A}^{-1}\mathbf{Z}_{i>j}'\mathbf{Z}_j,\sigma_j^2\mathbf{A}^{-1}\right). \tag{A.4}$$

To ameliorate computational burden, particularly for large N, we also adopts an exact sampling algorithm tailored for Gaussian priors, incorporating data augmentation as outlined in Bhattacharya, Chakraborty, and Mallick (2016). Algorithm 3 elaborates this methodology.

Algorithm 3 Sample sparse unconditional precision matrix $\mathbf{\Omega}$

Given initial hyperparameters for $\tilde{\lambda}_j^2$, $\mathbf{b}_{i>j}$, σ_j^2, and c,
for $j = 1 : N-1$ **do**
    Partition $\mathbf{Z}_{i>j}$ and $\mathbf{Z}_j$.
    Compute $\mathbf{D} = \text{diag}\left\{\frac{\lambda_j^2 \mathbf{b}_{i>j} c^2}{N^2 i} \frac{1}{\sigma_j^2}\right\}$ for $i > j$, $\mathbf{\Phi} = \sqrt{\sigma_j^2}\mathbf{Z}_{i>j}$, and $\mathbf{a} = \sqrt{\sigma_j^2}\mathbf{Z}_j$.
    Sample $\phi \sim \mathcal{N}(0, \mathbf{D})$, $v = \mathbf{\Phi}\phi + \mathcal{N}(0, \mathbb{I})$ and solve for w in $(\mathbf{\Phi D \Phi} + \mathbb{I})w = (\mathbf{a} - v)$.
    Given ϕ, $\mathbf{D}$, $\mathbf{\Phi}$, and w, sample $\boldsymbol{\beta}_{i>j} = u + \mathbf{D}\mathbf{\Phi}' w$.
    Sample $\lambda_j^2 \sim \mathcal{IG}\left(\frac{|i>j|}{2} + \frac{1}{2}, K_1\right)$, where $K_1 = \frac{1}{2}\boldsymbol{\beta}'_{i>j}\text{diag}\left\{\frac{N^2 i}{\sigma_j^2 \mathbf{b}_{i>j} c^2}\right\}\boldsymbol{\beta}_{i>j} + \frac{1}{a_j}$ for $i > j$.
    Sample $a_j \sim \mathcal{IG}\left(1, 1 + \tilde{\lambda}_j^{-2}\right)$.
    Sample $\mathbf{b}_{i>j} \sim \mathcal{IG}\left(1, K_2\right)$, where $K_2 = \frac{N^2 i}{2\sigma_j^2 \tilde{\lambda}_j^2 c^2}\boldsymbol{\beta}_{i>j} + \frac{1}{h_{i>j}}$ for $i > j$.
    Sample $h_{i>j} \sim \mathcal{IG}\left(1, 1 + \frac{1}{\mathbf{b}_{i>j}}\right)$.
    Sample $\sigma_j^2 \sim \mathcal{IG}\left(\frac{T+|i>j|}{2} + 0.01, K_3\right)$, where $K_3 = \frac{1}{2}\left\|\mathbf{Z}_j - \mathbf{Z}_{i>j}\boldsymbol{\beta}_{i>j}\right\|^2 + \frac{1}{2}\boldsymbol{\beta}'_{i>j}\text{diag}\left\{\frac{N^2 i}{\tilde{\lambda}_j^2 \mathbf{b}_{i>j} c^2}\right\}\boldsymbol{\beta}_{i>j} + 0.01$ for $i > j$.
    Update $L_{jj} = \sqrt{\sigma_j^2}$ and $L_{ij} = -\boldsymbol{\beta}_{i>j}/L_{jj}$ for $i > j$.
end for
Sample $\sigma_N^2 \sim \mathcal{IG}\left(\frac{N}{2} + 0.01, K_4\right)$, where $K_4 = 0.01 + \frac{1}{2}\left\|\mathbf{Z}_N\right\|^2$.
Update $L_{NN} = \sqrt{\sigma_N^2}$.
Compute $\mathbf{\Omega} = \mathbf{L}\mathbf{L}'$.

B Additional Empirical Results

B.1 Foreign Stock Price Indexes

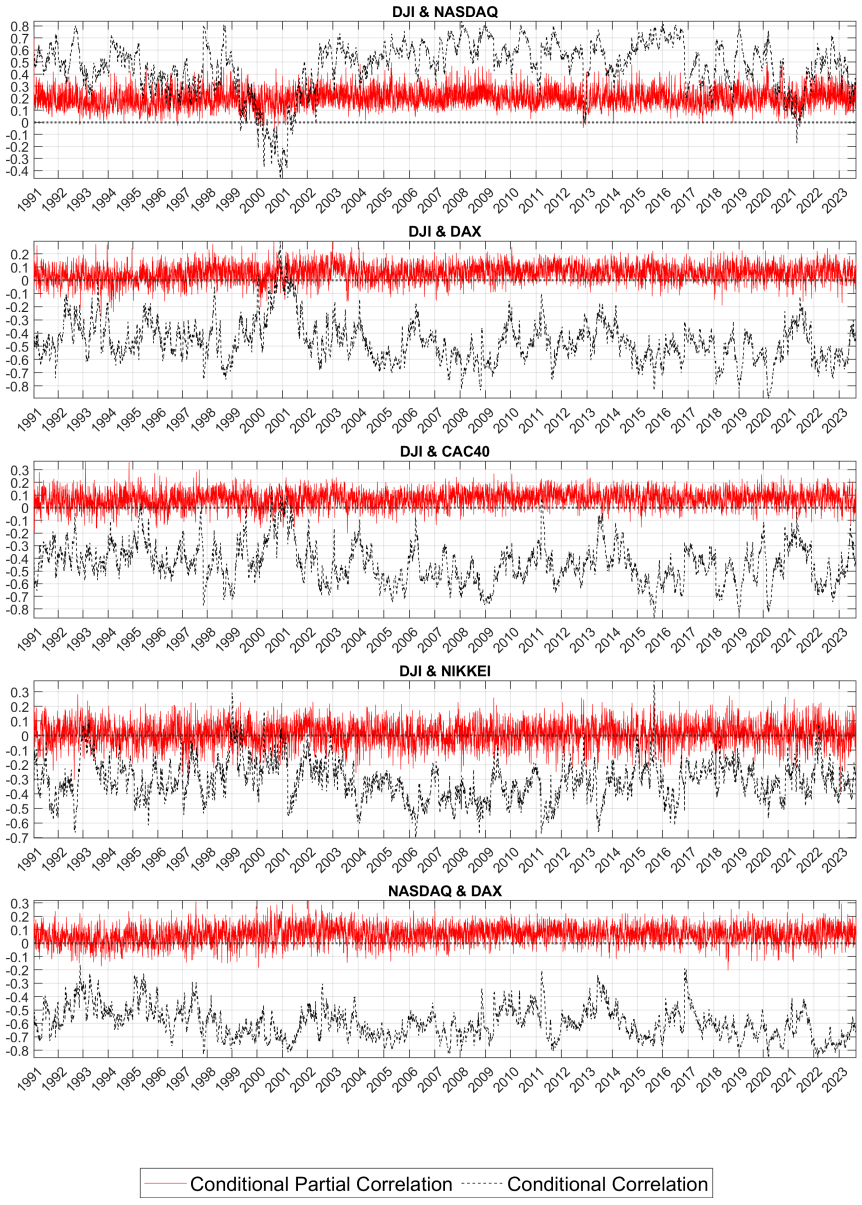

Figure B1: Dynamic Conditional (Partial) Correlations: Foreign Stock Indexes 1

Notes: The dataset has been sourced from Google Finance, spanning the period from January 4, 1991, to August 31, 2023. The measure for volatility is calculated using the formula: Volatility $= 100 \log(p_t/p_{t-1})$, where p_t represents the closing price of the respective stock index. The abbreviations for the stock indexes are as follows: DJI denotes the Dow Jones Industrial Average, NASDAQ signifies the National Association of Securities Dealers Automated Quotations, DAX stands for Deutscher Aktienindex, CAC40 is an acronym for Cotation AssistÃ©e en Continu 40, and NIKKEI represents the Nikkei 225 Stock Average.

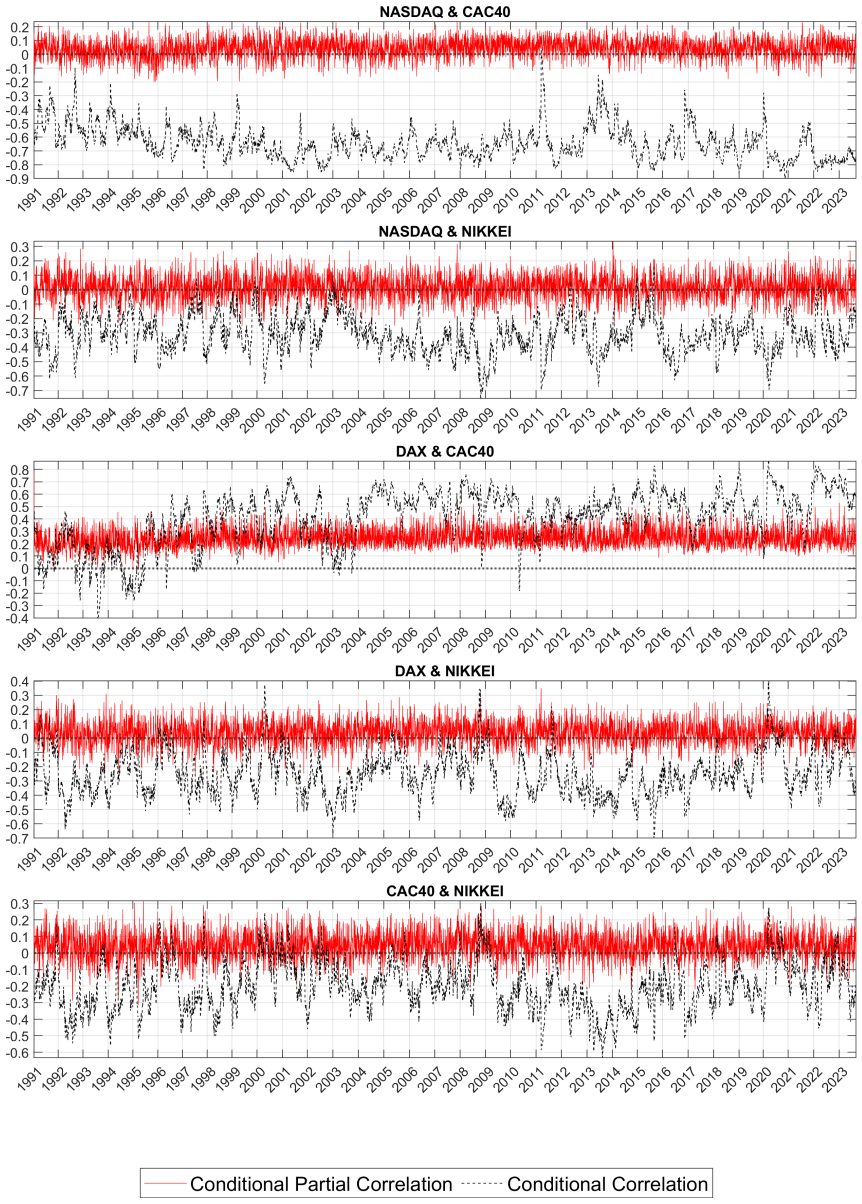

Figure B2: Dynamic Conditional (Partial) Correlations: Foreign Stock Indexes 2

Notes: The dataset has been sourced from Google Finance, spanning the period from January 4, 1991, to August 31, 2023. The measure for volatility is calculated using the formula: Volatility $= 100 \log(p_t/p_{t-1})$, where p_t represents the closing price of the respective stock index. The abbreviations for the stock indexes are as follows: DJI denotes the Dow Jones Industrial Average, NASDAQ signifies the National Association of Securities Dealers Automated Quotations, DAX stands for Deutscher Aktienindex, CAC40 is an acronym for Cotation AssistÃ©e en Continu 40, and NIKKEI represents the Nikkei 225 Stock Average.

B.2 Daily Returns on Securities Selected from S&P 500

The following figures delineate the conditional and partial correlation coefficients associated with the selected firms within each respective GICS sector.

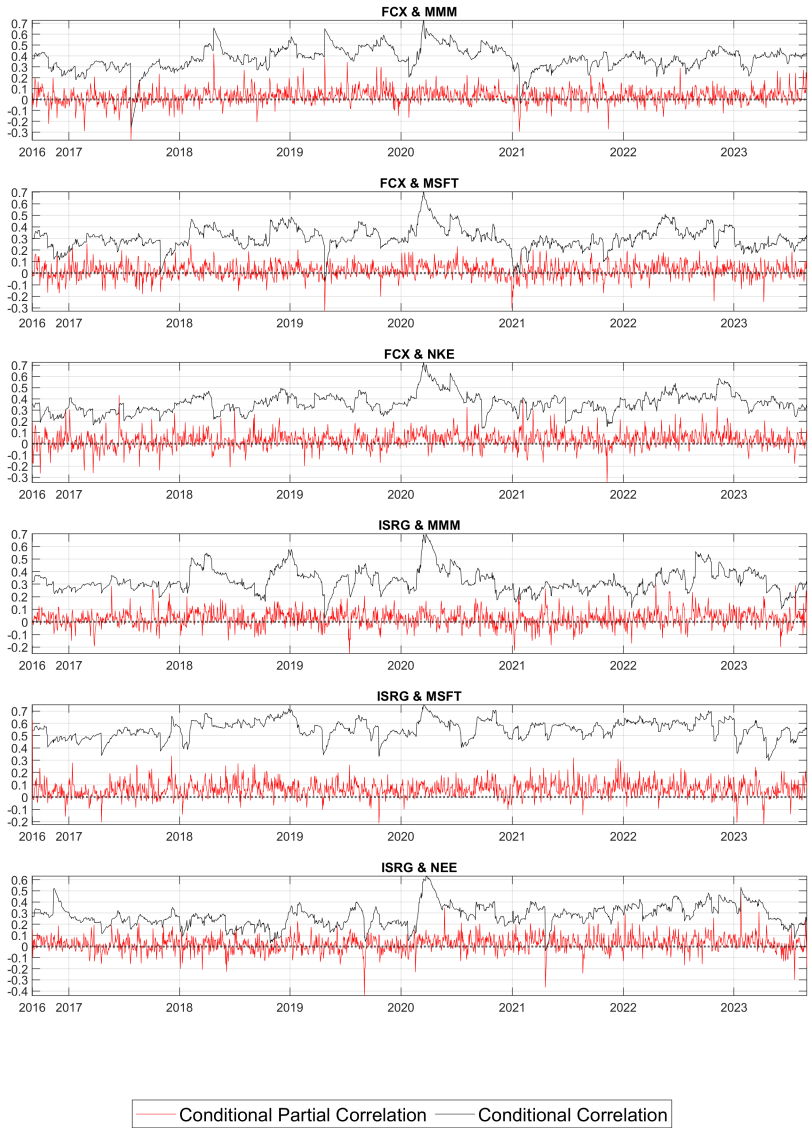

Figure B3: Dynamic Conditional (Partial) Correlations: Blue Chips Stocks from S&P 500 1

Notes: The figure describes the dynamic conditional correlations and dynamic conditional partial correlations among stock price volatilities for sectors characterized by a high degree of unconditional dependence. Stock ticker symbols corresponding to each sector are delineated as follows: Materials (FCX), Health Care (ISRG), Industrials (MMM), Information Technology (MSFT), Utilities (NEE), Communication Services (NFLX), Consumer Discretionary (NKE), Financials (SPG), Consumer Staples (WMT), and Energy (XOM). A comprehensive list of associated stock tickers can be found in Appendix C. To enhance visual representation, the dynamic conditional partial correlations have been scaled by a factor of 10.

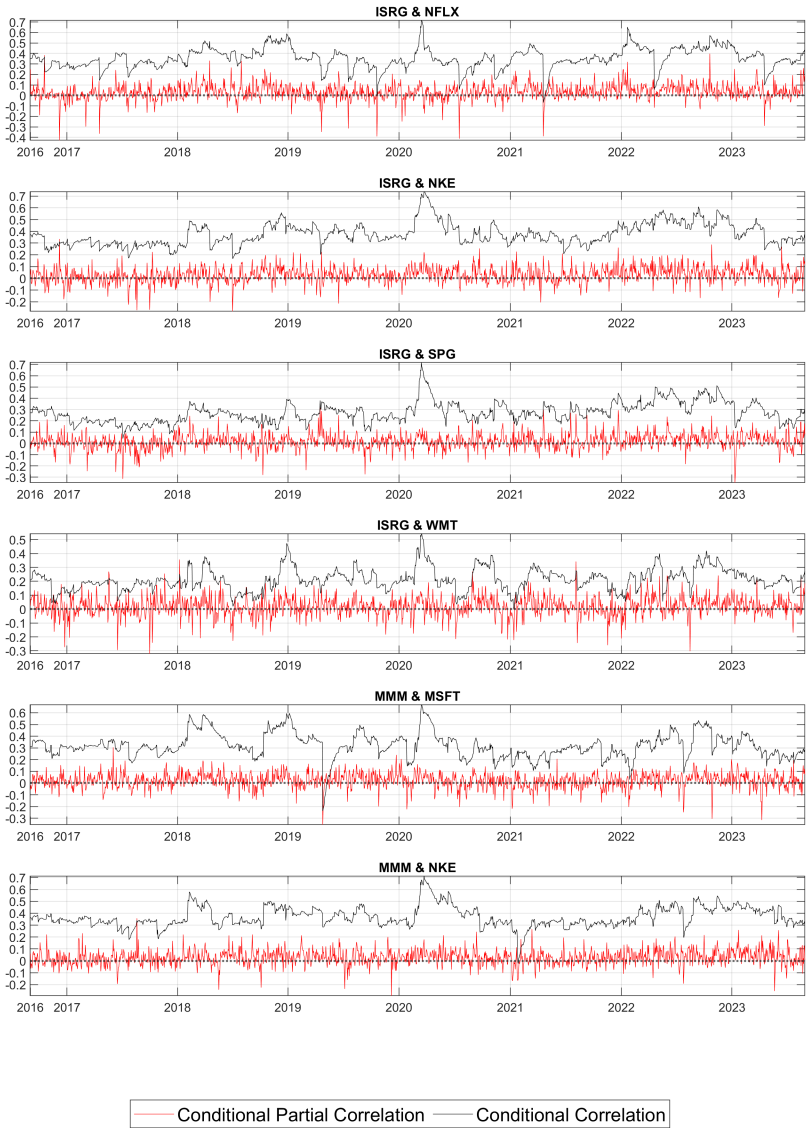

Figure B4: Dynamic Conditional (Partial) Correlations: Blue Chips Stocks from S&P 500 2

Notes: The figure describes the dynamic conditional correlations and dynamic conditional partial correlations among stock price volatilities for sectors characterized by a high degree of unconditional dependence. Stock ticker symbols corresponding to each sector are delineated as follows: Materials (FCX), Health Care (ISRG), Industrials (MMM), Information Technology (MSFT), Utilities (NEE), Communication Services (NFLX), Consumer Discretionary (NKE), Financials (SPG), Consumer Staples (WMT), and Energy (XOM). A comprehensive list of associated stock tickers can be found in Appendix C. To enhance visual representation, the dynamic conditional partial correlations have been scaled by a factor of 10.

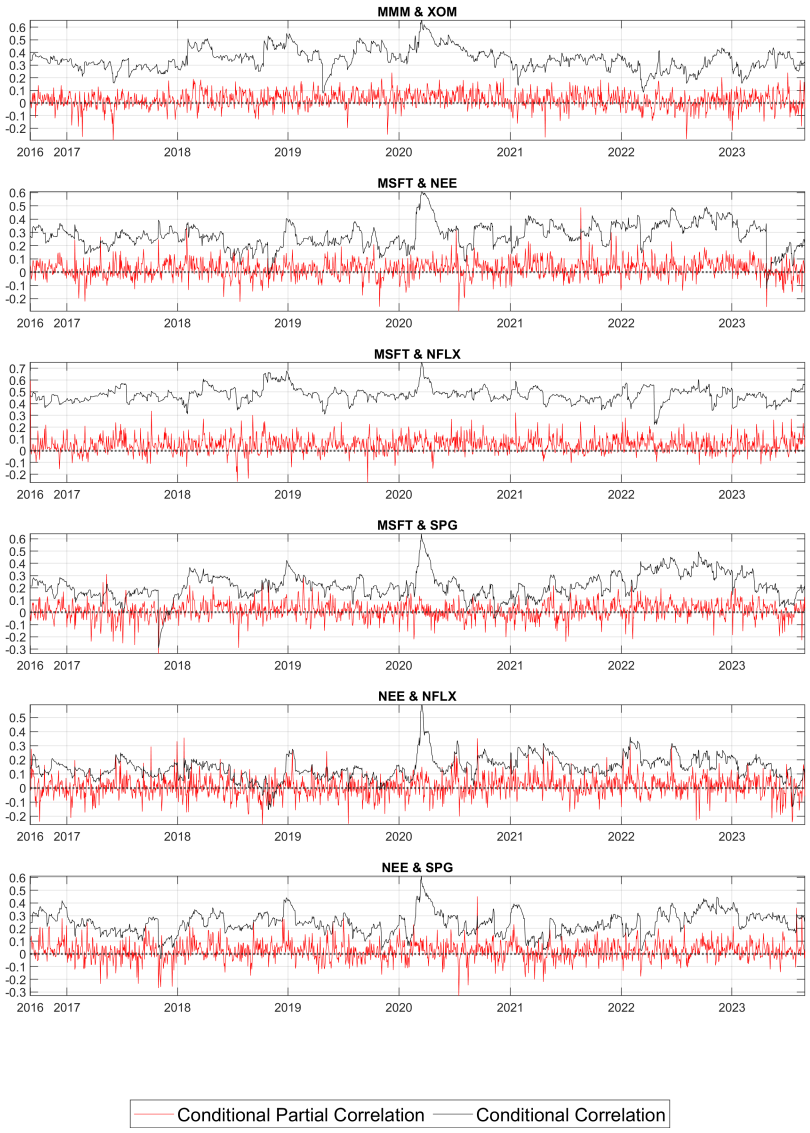

Figure B5: Dynamic Conditional (Partial) Correlations: Blue Chips Stocks from S&P 500 3

Notes: The figure describes the dynamic conditional correlations and dynamic conditional partial correlations among stock price volatilities for sectors characterized by a high degree of unconditional dependence. Stock ticker symbols corresponding to each sector are delineated as follows: Materials (FCX), Health Care (ISRG), Industrials (MMM), Information Technology (MSFT), Utilities (NEE), Communication Services (NFLX), Consumer Discretionary (NKE), Financials (SPG), Consumer Staples (WMT), and Energy (XOM). A comprehensive list of associated stock tickers can be found in Appendix C. To enhance visual representation, the dynamic conditional partial correlations have been scaled by a factor of 10.

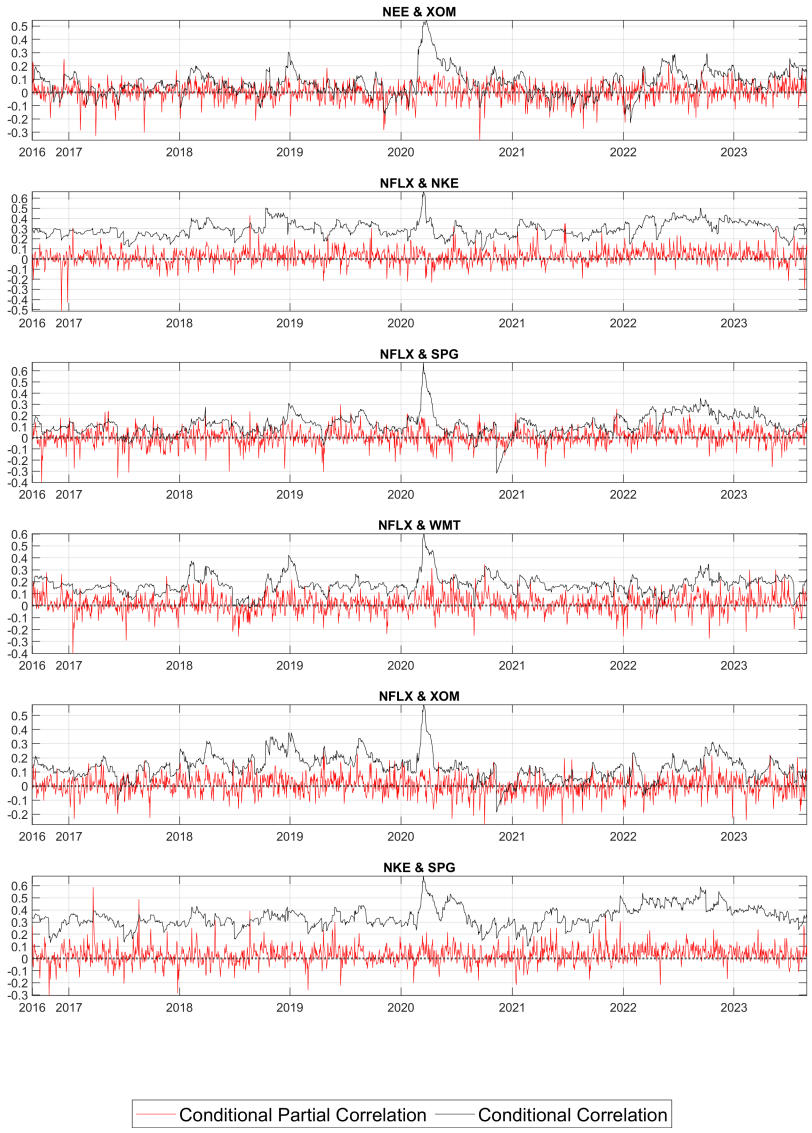

Figure B6: Dynamic Conditional (Partial) Correlations: Blue Chips Stocks from S&P 500 4

Notes: The figure describes the dynamic conditional correlations and dynamic conditional partial correlations among stock price volatilities for sectors characterized by a high degree of unconditional dependence. Stock ticker symbols corresponding to each sector are delineated as follows: Materials (FCX), Health Care (ISRG), Industrials (MMM), Information Technology (MSFT), Utilities (NEE), Communication Services (NFLX), Consumer Discretionary (NKE), Financials (SPG), Consumer Staples (WMT), and Energy (XOM). A comprehensive list of associated stock tickers can be found in Appendix C. To enhance visual representation, the dynamic conditional partial correlations have been scaled by a factor of 10.

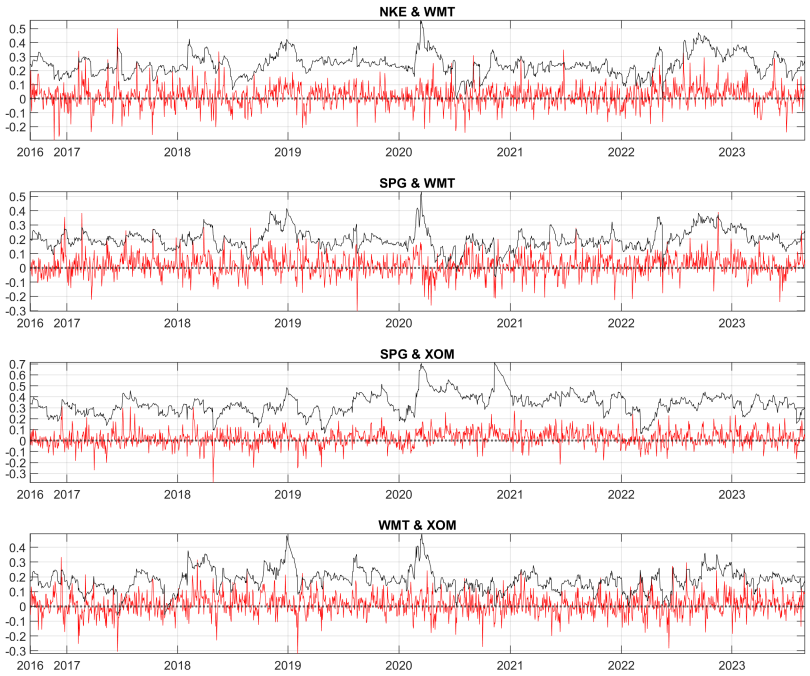

Figure B7: Dynamic Conditional (Partial) Correlations: Blue Chips Stocks from S&P 500 5

Notes: The figure describes the dynamic conditional correlations and dynamic conditional partial correlations among stock price volatilities for sectors characterized by a high degree of unconditional dependence. Stock ticker symbols corresponding to each sector are delineated as follows: Materials (FCX), Health Care (ISRG), Industrials (MMM), Information Technology (MSFT), Utilities (NEE), Communication Services (NFLX), Consumer Discretionary (NKE), Financials (SPG), Consumer Staples (WMT), and Energy (XOM). A comprehensive list of associated stock tickers can be found in Appendix C. To enhance visual representation, the dynamic conditional partial correlations have been scaled by a factor of 10.

C List of Companies

Table C1 lists the blue chip stocks incorporated into the empirical analysis in Section 5.2 selected from S&P 500 companies.

Table C1: List of Companies used in Section 5.2

Ticker	Company	GICS (Sector)	Ticker	Company	GICS (Sector)
AAPL	Apple Inc.	Information Technology	IBM	International Bus. Machines	Information Technology
ABBV	AbbVie	Health Care	INTC	Intel Corp.	Information Technology
ABT	Abbott Laboratories	Health Care	INTU	Intuit Inc.	Information Technology
ACN	Accenture plc	Information Technology	ISRG	Intuitive Surgical, Inc.	Health Care
ADBE	Adobe Inc.	Information Technology	JNJ	Johnson & Johnson	Health Care
AEP	American Electric Power	Utilities	JPM	JPMorgan Chase & Co.	Financials
AIG	American International Group	Financials	KO	The Coca Cola Company	Consumer Staples
ALL	Allstate Corp	Financials	LLY	Lilly (Eli) & Co.	Health Care
AMGN	Amgen Inc.	Health Care	LMT	Lockheed Martin Corp.	Industrials
AMZN	Amazon.com Inc.	Consumer Discretionary	LOW	Lowes Cos.	Consumer Discretionary
APA	Apache Corporation	Energy	MCD	McDonalds Corp.	Consumer Discretionary
AXP	American Express Co.	Financials	MDLZ	Mondelez International	Consumer Staples
BA	Boeing Company	Industrials	MDT	Medtronic Inc.	Health Care
BAC	Bank of America Corp	Financials	MET	MetLife Inc.	Financials
BAX	Baxter International Inc.	Health Care	META	Meta Platforms Inc.	Information Technology
BK	The Bank of New York Mellon Corp.	Financials	MMM	3M Company	Industrials
BMY	Bristol-Myers Squibb	Health Care	MO	Altria Group Inc.	Materials
C	Citigroup Inc.	Financials	MRK	Merck & Co.	Health Care
CAT	Caterpillar Inc.	Industrials	MS	Morgan Stanley	Financials
CL	Colgate-Palmolive	Consumer Staples	MSFT	Microsoft Corp.	Information Technology
CMCSA	Comcast Corp.	Consumer Discretionary	NEE	NextEra Energy Inc.	Utilities
CME	CME Group Inc.	Financials	NFLX	Netflix Inc.	Communication Services
COF	Capital One Financial	Financials	NKE	NIKE Inc.	Consumer Discretionary
COP	ConocoPhillips	Energy	NOV	National Oilwell Varco Inc.	Energy
COST	Costco Co.	Consumer Staples	NSC	Norfolk Southern Corp.	Industrials
CRM	Salesforce Inc.	Information Technology	ORCL	Oracle Corp.	Information Technology
CSCO	Cisco Systems	Information Technology	OXY	Occidental Petroleum	Energy
CVS	CVS Caremark Corp.	Consumer Staples	PEP	PepsiCo Inc.	Consumer Staples
CVX	Chevron Corp.	Energy	PFE	Pfizer Inc.	Health Care
DD	Du Pont (E.I.)	Materials	PG	Procter & Gamble	Consumer Staples
DELL	Dell Technologies Inc.	Information Technology	PM	Philip Morris International	Consumer Staples
DIS	The Walt Disney Company	Consumer Discretionary	QCOM	QUALCOMM Inc.	Information Technology
DVN	Devon Energy Corp.	Energy	RTN	Raytheon Co.	Industrials
EBAY	eBay Inc.	Information Technology	SBUX	Starbucks Corp.	Consumer Discretionary
EMR	Emerson Electric	Industrials	SLB	Schlumberger Ltd.	Energy
EXC	Exelon Corp.	Utilities	SO	Southern Co.	Utilities
F	Ford Motor	Consumer Discretionary	SPG	Simon Property Group Inc	Financials
FCX	Freeport-McMoran Cp & Gld	Materials	T	AT&T Inc.	Communication Services
FDX	FedEx Corporation	Industrials	TGT	Target Corp.	Consumer Discretionary
GD	General Dynamics	Industrials	TXN	Texas Instruments	Information Technology
GE	General Electric	Industrials	UNH	United Health Group Inc.	Health Care
GILD	Gilead Sciences	Health Care	UNP	Union Pacific	Industrials
GM	General Motors	Consumer Discretionary	UPS	United Parcel Service	Industrials
GOOG	Google Inc.	Information Technology	USB	U.S. Bancorp	Financials
GS	Goldman Sachs Group	Financials	V	Visa Inc.	Information Technology
HAL	Halliburton Co.	Energy	VZ	Verizon Communications	Information Technology
HD	Home Depot	Consumer Discretionary	WFC	Wells Fargo	Financials
HON	Honeywell Intl Inc.	Industrials	WMT	Wal-Mart Stores	Consumer Staples
HPQ	Hewlett-Packard	Information Technology	XOM	Exxon Mobil Corp.	Energy